RSC Advances

ROYAL SOCIETY OF CHEMISTRY

www.rsc.org/advances

State of the art of the nanoforest structures and their applications.

Boris I. Kharisov, Oxana V. Kharissova,* Beatriz Ortega García,
Yolanda Peña Méndez, Idalia Gómez de la Fuente

Universidad Autónoma de Nuevo León, Monterrey, México.
Corresponding author. E-mail bkhariss@hotmail.com

Abstract

Forest-like nanostructures, their synthesis, properties, and applications are reviewed. Nanoforests are mainly represented by carbon nanotubes, zinc and titanium oxides, and gold, much lesser by other metals, metal oxides, arsenides and phosphides. These nanostructures generally consist of more simple 1D objects, such as nanowires, nanopillars, nanorods, nanotrees, nanofibers or nanotubes. Synthesis methods for nanoforests vary from catalytic pyrolysis or thermal decomposition of hydrocarbons to electrophoretic deposition, hydrothermal route, electron beam lithography, focused-ion-beam technique, vapor phase transport, facet-selective etching and pulsed deep reactive etching technologies, among others. A row of applications for the forest-like nanostructures are generalized, for instance as sensors / detectors, photoanodes in solar and fuel cells, supercapacitors and energy storage devices, SERS applications, optical and MEMs switching devices, water splitting processes, CO_2 fixation, and as supports / targets for biomolecules. In general, it is expected that more varieties of compounds and materials with exciting properties can be obtained in this form in near future, thus expanding numerous applications of forest-like nanostructures.

Keywords: Nanoforest, nanotree, nanowires, carbon nanotubes, zinc oxide, titanium dioxide, protein nanoforests.

Introduction

"Nanoforests", or "forest-like nanostructures", as a conglomerate of nanotrees and nanobushes and other "nanovegetation"-like nanostructures, as well as simple nanorods, nanopillars, nanowires, nanobars, nanoneedles, nanobelts and other relative 1D nanostructures, have been reported mainly for carbon nanotubes,[1] although they are known for a few metal oxides (for example ZnO[2] and TiO_2[3]) or organic nanoforests of peptide nanotubes.[4] It is known that 1D nanostructures above are nowadays emerging materials, possessing extraordinary properties and a variety of applications, in particular in nanophotonic and optoelectronic devices. So, their agglomerations could be much more effective in comparison with 1D precursors, in particular due to an increased surface area.[5] That´s why a series of novel applications have been found for nanoforests, for instance for preparation of solderless and durable electrical contacts,[6] in the area of photovoltaic devices[7] and thermoelectric uses.[8] It is also well-known that 1÷3D nanomaterials are widely applied as catalysis in a variety of processes,[9 10 11 12 13] in particular for methanol oxidation.[14 15 16 17] In this respect, current and future achievements in novel catalytic processes on nanoforest basis could be a big-foot step in further development of this field.

Comprehensive reviews on nanotechnology, containing sections on nanoforests with particular covered aspects, have been recently published.[18 19] In this review, we present

a concise state of the art of this type of nanostructures, their preparation, peculiarities, and current applications, taking into account that nanoforests (except those of CNTs) can be still considered as relatively rare morphology, although very promising.

Most common nanoforests

Carbon nanotube forests (CNTFs)

The nanoforests on the basis of carbon nanotubes belong indubitably most studied forest-like structures among other compounds, whose number is certainly limited, and have got useful applications. The CNTFs´ peculiarity, in comparison with other carbon and non-carbon species, is that the forests of carbon nanotubes are currently known as the darkest artificially produced materials,[20] being able to adsorb the entire visible range of electromagnetic wave much more efficiently than any other black material. They exhibit near-perfect optical absorption (reflectance~0.045%) due to low reflectance and nanoscale surface roughness. At the same time, carbon nanotubes are able to reflect light like a mirror when the CNTs in the forests are mechanically bent and flattened with proper control.[21] Under a controlled mechanical processing of the CNTs, the mirror-like reflection from the processed area with 10%–15% reflectivity was observed, having possible applications for fabrication of monolithically integrated reflector-absorber arrays.

Carbon nanotube forests may include ”regular”,[22] bamboo-like,[23] helical[24] and branched structures, as well as a CNT forest-on-forest, where the number of layers in such a system can vary from one[25] to two,[26] four,[27] eight[28] and even forty,[29] and second- and third-order CNT forest structures.[30 31] Integrated simulation of active carbon nanotube forest growth, the diverse CNT forest morphologies, and mechanical compression is discussed in a recent report.[32] In particular, CNT forest morphologies may be generally aligned to the growth axis or highly tortuous, with persistently wavy CNTs intermixed with aligned and straight carbon nanotubes. This depends on the height of CNT forest, the CNT diameter, surface density, and growth conditions. The length of some CNTs may exceed the height of the carbon nanotube forest; different CNTs in the same nanotube forest can be different in tortuosity and length. Comprehensive information on CNTs forests is present in a highly recommended excellent comprehensive recent review,[33] citing 679 references. This shows an increasing interest to this type of nanostructure having a variety of applications, from catalysis to biosensors.

Synthesis. In general, CNTs forests can be synthesized by catalytic pyrolysis on supported catalysts as described below; using various versions of the CVD method;[34 35 36] by the template method with Al_2O_3 membranes; by graphite sputtering (this technique is used much more rarely), by electrophoresis or dielectrophoresis of CNTs from dispersions[37 38] and by chemical grafting of CNTs onto substrates.[39] Particular aspects of methods for the synthesis of CNTFs are mentioned in several reviews.[40 41] Among them, we note a wide use of mono- and polymetallic catalysts and supports for their preparation, mainly at high temperatures and using acetylene as carbon source {although ethylene mixtures with H_2[42] (the equipment is shown in Fig. 1) or $C_2H_4/H_2/H_2O/Ar$[43] were used}. Thus, the growth of dense CNT forests on some metallic layers (Mo, Ta, W, and Ir) by thermal decomposition of C_2H_2 diluted in NH_3 was studied.[44] The growth process and resulting structure of CNT forests were shown to

depend on metal substrates, process duration, temperature, and thickness of the stabilizer (Al). In a related report,[45] dense CNTs forests (height of ~300 nm and a mass density of 1.2 $g \cdot cm^{-3}$) were prepared on copper support at 450°C, using Co/Al/Mo multilayer catalyst. The nanotubes exhibited very narrow inner spacing. Main characteristics of the formed material are high thermal effusivity and a thermal conductivity, suitable for possible uses in heat dissipation devices. Another classic example consists of vertically aligned SWCNTs forest, grown using FePt alloy particles on a MgO substrate.[46] Sometimes, metal-based catalyst should be additionally activated prior to use. Thus, an oxidative pretreatment of Fe, Co, or Ni growth catalyst on SiO_2 support can be used to switch the growth mode of CNTs from tip growth to root growth.[47] Dense vertically aligned nanotube forests can be grown this way. The oxidative treatment effect was explained by appeared strong interaction "catalyst-support (SiO_2)", limiting the surface diffusion, sinterization of catalyst NPs, and their binding to the surface of SiO_2. In addition, vertically aligned small diameter (single- and few-walled) carbon nanotube forests were also grown by thermal CVD over the temperature range 560-800°C and 10^{-5} to 14 mbar partial pressure range, using acetylene as the feedstock and Al_2O_3-supported Fe nanoparticles as the catalyst.[48] Following mechanism of their formation (Fig. 2) is described by reactions (*1*-*5*); alternative mechanism is shown in Fig. 3.[49] Curiously (Fig. 3G), nanoforest zones consisting of sinuous (Fig. 3G, left section, up) and almost straight (Fig. 3G, right section, down) carbon nanotubes can be sometimes formed at the same bulk growth conditions.

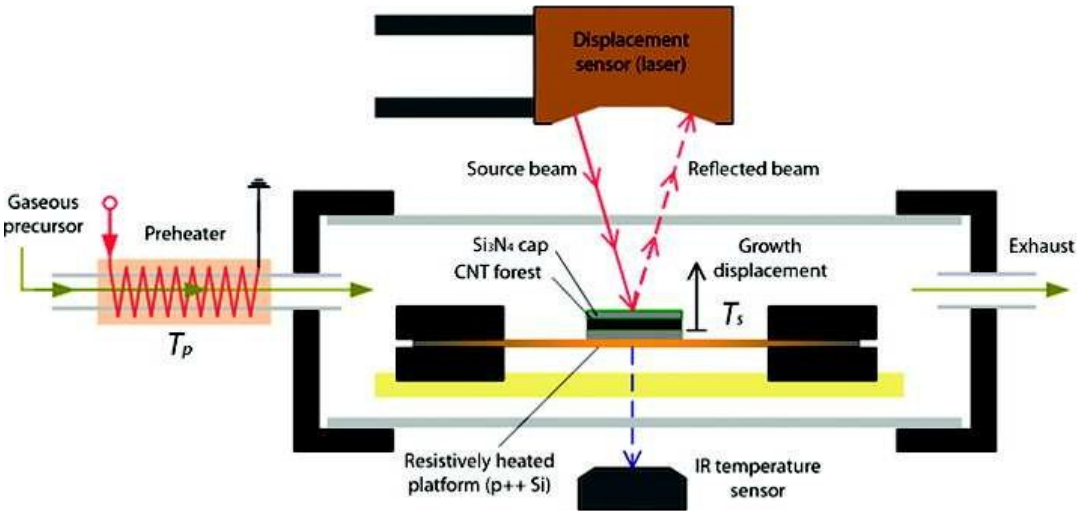

Fig. 1. Obtaining CNTs forest by CVD method. Reproduced with permission of the *American Chemical Society.*

$$C_2H_{2\ gas} \leftrightarrow C_2H_{2\ ads} \quad (1)$$
$$C_2H_{2\ ads} \leftrightarrow 2CH_{ads} \quad (2)$$
$$CH_{ads} \leftrightarrow C_{ads} + H_{ads} \quad (3)$$
$$2H_{ads} \rightarrow H_{2gas} \quad (4)$$
$$C_{ads} \rightarrow C_{CNT} \quad (5)$$

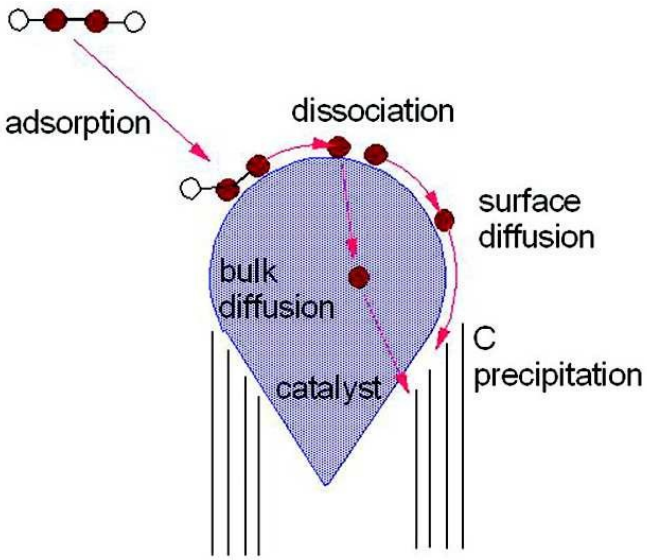

Fig. 2. Schematic of CNT growth process. Copyright. Reproduced with permission of the *American Chemical Society.*

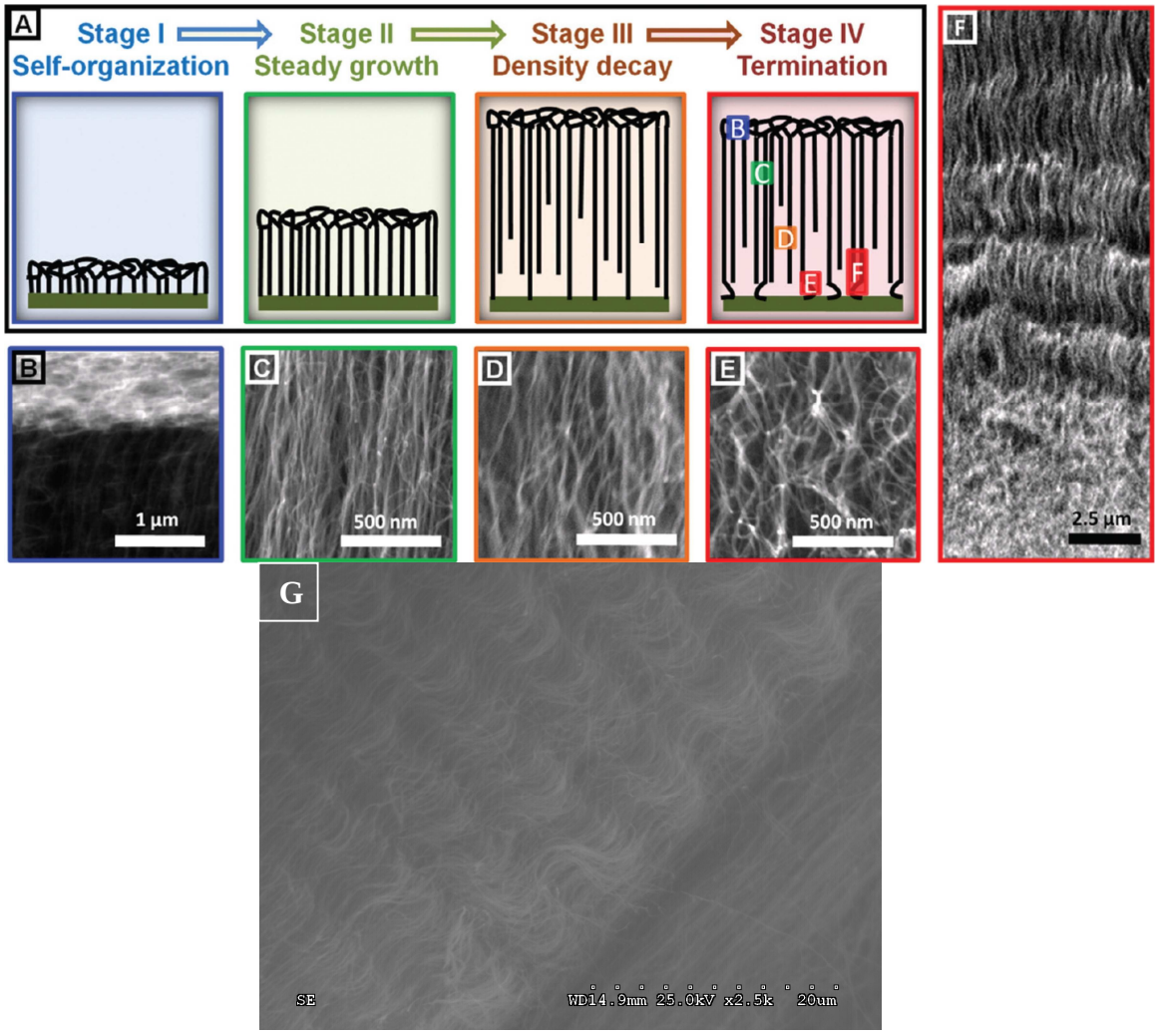

Fig. 3. Collective growth mechanism of a CNT forest: (A) growth stages and SEM images of (B) tangled crust at the top of forest, (C) aligned and dense morphology near the top of a self-terminated forest, (D) less aligned and less dense morphology in the

lower region of a self-terminated forest, and (E, F) randomly oriented morphology at the bottom, induced by the loss of the self-supporting forest structure. Reproduced with permission of the *American Chemical Society*. (G) View of a coexistence of sinuous-like and almost straight carbon nanotubes in the same image (authors' own data).

Additionally to metals above as supports, CVD-assisted formation of a dense CNTs (length 13-14 mm and diameter of 10-100 nm) forest is known using spin-coated iron oxide (Fe_2O_3) thinfilm on Si substrate starting from a mixture of acetylene, hydrogen and nitrogen for 45 min at 700°C.[50] Also, vertically aligned ohmic-conductive carbon nanotube forests were grown on TiSiN refractory conductive films and reached area densities of $(5.1\pm0.1)\times10^{12}$ tubes cm^{-2} and mass densities of approximately 0.3 $g{\cdot}cm^{-3}$.[51] The above support had a function as a diffusion barrier; the resulting nanoforest grew according to the root growth mechanism. An additional discontinuous AlO_x layer, inhibiting catalyst nanoparticle sintering, allowed maximizing the CNTs area density.

To optimize high-temperature growth of CNTFs, several studies have been carried out, since an important obstacle of CNTs fabrication in industrial mass production is the growth efficiency. Thus, for the case of C_2H_2 as precursor in water-assisted CVD, it was established[52] that, for 10 min. optimum growth conditions, SWCNT forests with ~350 μm/min initial growth rates, ~2500 μm height, and extended catalyst lifetimes could be reached by increasing the dwell time to ~5 s. It demonstrated the generality of dwell time control to highly reactive gases. In another research, in order to tune the CVD-growth of CNTs forests (DWCNTs or SWCNTs) on wafers, introduction of CO_2 is a simple and controlled way.[53] When its concentration grows, the CNTs forests are transformed as follows: CNTs forests → radial blocks → bowl-shaped forests. It is possible to control the diameter distribution and wall number of the CNTs this way. At 36.8 mol% of CO_2, the content of SWCNTs in the forest was found to be 70%. Also, under increased CO_2 concentration, a smaller diameter and decreased wall number for CNTs were revealed. It was suggested that CO_2 could be as a weak oxidant and generates water. Among other synthesis methods[54] for CNTFs, we note high voltage electrophoretic deposition (HVEPD), used to obtain forests of aligned MWCNTs on long strips of conductive substrates.[55]

Special studies of CNTFs internal structure and other properties. XPS analysis of a CVD-grown forest of MWCNTs using monochromatic Al Kα radiation showed essentially only carbon presence (1s peak at 284.5 eV).[56] In order to evaluate properties of the "internal content" of CNTFs, the precise and continuous control method for the average diameter of SWCNTs in a forest ranging from 1.3 to 3.0 nm with 1 Å resolution was offered.[57] This control was reached through tuning of the catalyst state (composition, size, and density) applying arc plasma deposition of nanoparticles. These results showed a direct relationship between the achievable height and the diameter of SWCNTs. On their basis, the fundamental difficulty in fabrication of tall and small diameter SWCNT forests was suggested. In addition, the internal nanostructure of the CNTs forest, consisting of mostly empty space between the nanotubes, allows capture photons effectively, yet allows electrons to escape easily (Fig. 4).[58] This makes possible to use CNTS forests in ranging from photocathodes to solar cells.

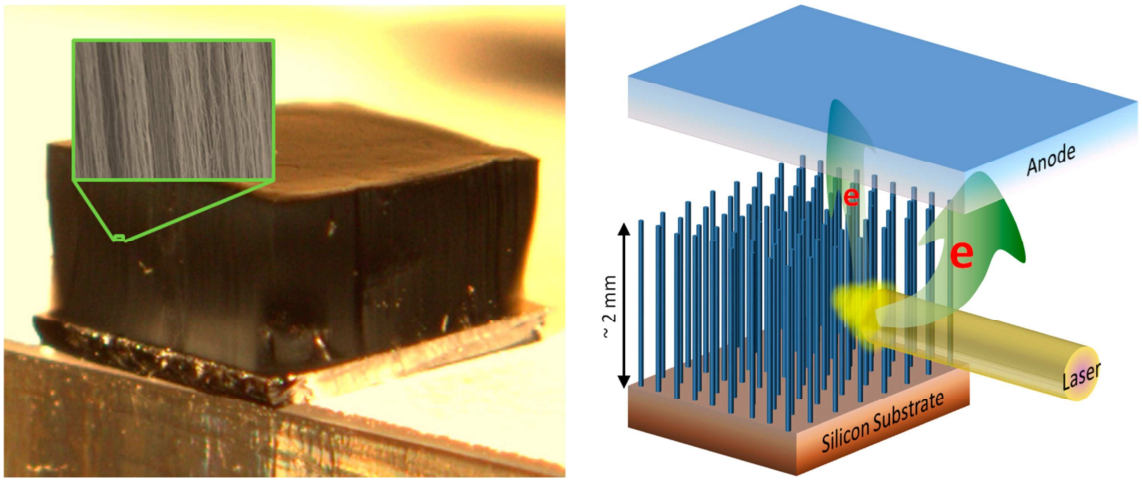

Fig. 4. (Left) A photo of a carbon nanotube forest over 2 mm tall and 5 mm on each side (note the silicon substrate with a thickness of 0.5 mm), effectively forming a macroscopic object. Inset is a scanning electron micrograph of the sidewall of the forest, showing the overall alignment of the nanotubes and the significant internanotube distance. (Right) A schematic of the experiment, showing the electrons exiting from the sidewall of the forest, as well as those emerging from the top surface of the forest. Reproduced with permission of the *American Chemical Society.*

Vertically aligned CNTs possess a peculiarity of *waviness*, regardless of the control of their fabrication process. Study of this phenomena showed[59] that the inherent waviness is the main mechanism by which the effective modulus of CNTs is reduced by several orders of magnitude. The high compliance of forests of carbon nanotubes was found to be because of the inherent waviness of individual CNTs, and not necessarily due to bending and buckling of CNTs. The *mechanical compression effect* on the thermal conductivity of the closely-aligned parallel SWCNTs forest was investigated by molecular dynamics simulations.[60] Among other findings, the thermal conductivity was shown to be linearly enhanced by increasing compression before the buckling of SWCNT forests. At the same time, the thermal conductivity decreases quickly with further increasing compression after the forest is buckled. The intertube van der Waals interaction is strengthened by the compression and the smoothness of the inter-tube interface is maintained during compression. In addition, *buckling-driven delamination* of CNTs forests from their growth substrates when subjected to compression was revealed.[61] It was postulated that the post-buckling tensile stresses, being developed at the base of the CNT forests, serve as the driving force for delamination. Also, the fundamental dependence *electrical conductance* and *thermal diffusivity* on the diameter and defect level for aligned SWCNTs forests (fabrication scheme see Fig. 5) was evaluated.[62] It was definitively concluded that high thermal diffusivity and electrical conductance would be extremely difficult to simultaneously reach by a single SWCNT forest structure using CVD technique.

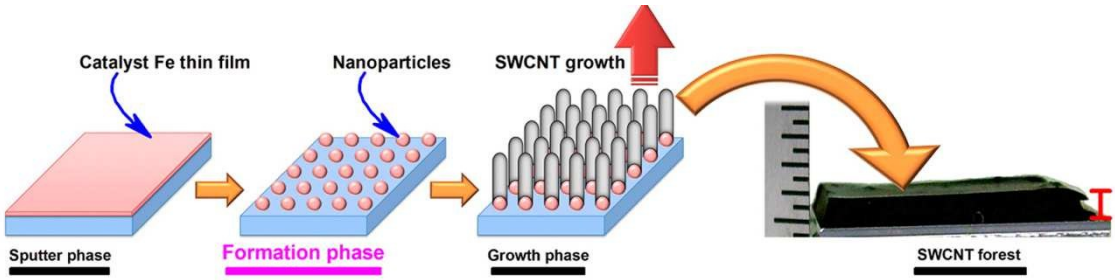

Fig. 5. Schematic of synthesizing SWCNT forests by tailoring Fe thin film thickness and formation temperature. Reproduced with permission of the *American Chemical Society.*

Liquid flow slippage over superhydrophobic surfaces made of CNTs forests, incorporated in microchannels, was also studied.[63] We need to note that CNTFs composites with highly hydrophobic properties can be created by special methods. Thus, a stable superhydrophobic surface was created using the nano-scale roughness inherent in a vertically aligned CNTs forest.[64] This became possible due to the use of a thin conformal hydrophobic polytetrafluoroethylene (PTFE), which coated the surface of the CNTs. In this material, essentially spherical, micrometer-sized water droplets can be suspended on top of the CNTs forest. This effect could be explained on the basis that that the appearing difluorocarbene radicals may attach covalently to the nanotube surface and subsequently polymerize from these sites. The product could get several applications, in particular as fillers for nanocomposites and single strand conductors in molecular electronics. Among other important studies, we mention the linearized Gouy-Chapman-Stern theory of an electric double layer, generalized for morphologically complex and disordered electrodes,[65] in particular its significance was illustrated for a forest of nanopillars. The theory allows analyzing the effect of compact layer thickness, concentration, shapes and their fluctuations, developing a general understanding of capacitance in complex interfacial systems.

Applications of CNTFs and their composites belong to a variety of areas, from academic to technical and medicinal. Thus, CNTs nanoforests, each with a thin conformal coating of dielectric, can provide an economic fabrication of sensitive and uniform SERS templates.[66] CNTFs are also considered as particularly promising templates for the formation of porous metal oxides (Al_2O_3, TiO_2, V_2O_5 and ZnO).[67] A bi-layer Au-carbon nanotube composite (a vertically aligned MWCNTs forest, sputtered with an Au layer) was fabricated as a potential low-force electrical contact surface for possible applications in MEMs switching devices.[68] The penetration of Au atoms into the forest directly influences the electrical characteristics of the composite, depending on loading conditions (the effective resistivities are in the range from 303 nΩ m down to 54 nΩ m).

Sensing uses are also common. Thus, a unique combination process of a sharp Si microneedle array and MWCNT forest was developed and applied a reference electrode for a non-enzymatic glucose sensing.[69] The registered sensivity was found to be 17.73±3 μA/mM-cm^2. This electrode can be used for painless diabetes testing applications. Also, carbon nanofiber forests (CNFFs) grown on glass microballoons are able to detect directly *Plasmodium falciparum* histidine rich protein-2 (PfHRP-2) antigen as low as 0.025 ng/mL concentration in phosphate buffered saline.[70] This effect can be applied for early diagnosis of malaria and other infectious diseases. Among technical applications, CNTs forests have been revealed to reduce the access of abrasive particles to compressible sealing elements of joints.[71] In addition, a spray-based coating technique was applied for deposition of nanoscale coatings of polystyrene and poly-3-hexylthiophene onto carbon nanotube forests, being as a bonding medium that produces thermal resistance by expanding the area available for heat transfer at CNT contacts.[72]

Diamond-based nanoforests are known, in addition to CNTFs and CNFFs above. Thus, an electrode with 3D structure on the basis of boron-doped diamond nanorod forest

(BDDNF) was fabricated by hot filament CVD method (HFCVD) method (Fig. 6).[73] In its preparation, the electroless metal deposition (EMD) method and HFCVD technique were combined for growing the BDDNF on Si nanowires; as a result, a 2D B-doped diamond electrode was transformed to 3D analogue. This electrode was found to exhibit a better selectivity and sensivity for biomolecule detection (for example, for glucose oxidation in basic conditions) in comparison with conventional planar B-doped diamond electrodes.

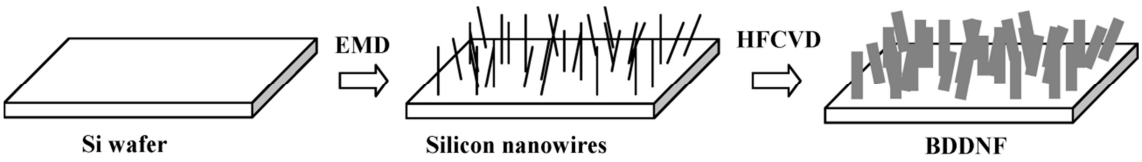

Fig. 6. Plots of fabrication of the BDDNF. Reproduced with permission of the *American Chemical Society.*

Zinc oxide nanoforests

Hydrothermal-assisted synthesis. Zinc oxide, an extraordinary compound in nanotechnology, which can exist in a huge variety of structural types, from classic to less-common, is widely presented in the forest-like forms, similarly to the CNTFs above. The ZnO nanoforests can be prepared by a series of techniques, mainly by the hydrothermal route;[74] the methods for the controlled growth of ZnO nanowires, leading, in particular, to nanoforests formation, are reviewed in.[75] In a typical synthesis, 3D ZnO willow-like nanoforests (Fig. 7) were prepared *via* a facile hydrothermal route using ZnO nanobranches onto preformed ZnO nanowire arrays, thus representing a wonderful morphology-controlled synthesis, tuning systematically ammonia and PEI (polyethylenimine) concentrations, influencing on the architecture of ZnO nanoforests.[76] This unique product has prominent PEC water splitting performance: a high photoconversion efficiency of 0.299% at 0.89 V (vs. RHE) was observed. In a related report,[77] the high density nanoforest containing long branched tree-like multigeneration hierarchical ZnO nanowire photoanodes was hydrothermally fabricated (Figs. 8-9). For this branched material, the light conversion was found to be 5 times more than the efficiency of the materials based on upstanding ZnO nanowires, due to highly enhanced surface area and reduced charge recombination. Additionally, flexible solar cells could be made using thus obtained nanoforest. In addition, the hydrothermal methods can be united with other techniques, as, for example, it was reported[78] for the *electron beam lithography* (EBL). The EBL in combination with subsequent hydrothermal synthesis (Figs. 10-11) was applied to fabricate patterned ZnO nanorod arrays with different spacing distances and densities on silicon (Si) substrate. The geometric parameters of ZnO nanorod arrays can be expediently controlled in this process. The purpose of the EBL use was to fabricate the patterned ZnO seed layers with different spacing distances and areas with high precise; the next step, a hydrothermal growth method, was used to control the density and morphologies of ZnO nanorod arrays. Such a combination allows integration of patterned arrays into real devices.

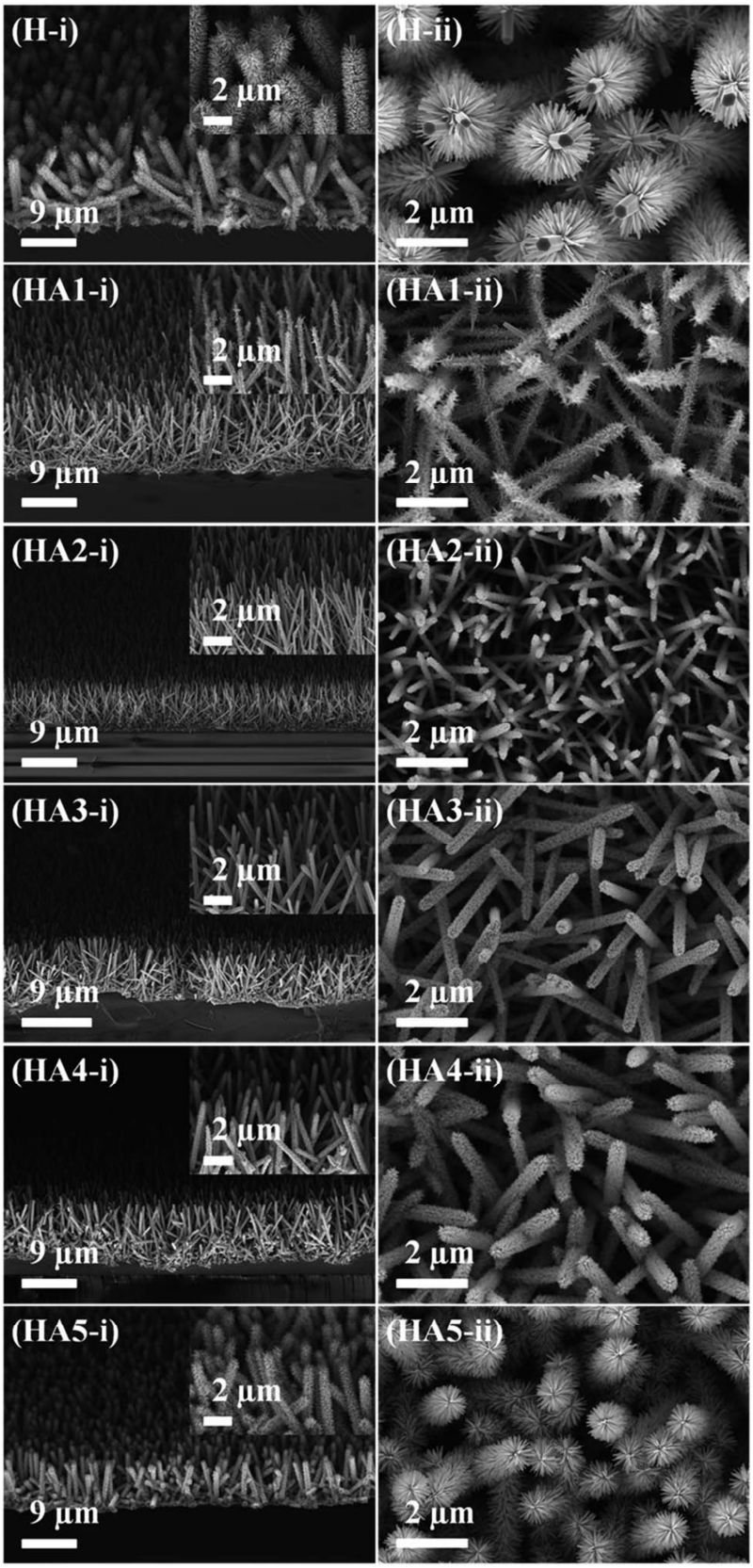

Fig. 7. SEM images of the obtained ZnO nanoforests after growing ZnO nanobranches onto the preformed ZnO nanowire arrays in precursor solutions with different concentrations of ammonia but without PEI. Reproduced with permission of the *Royal Society of Chemistry.*

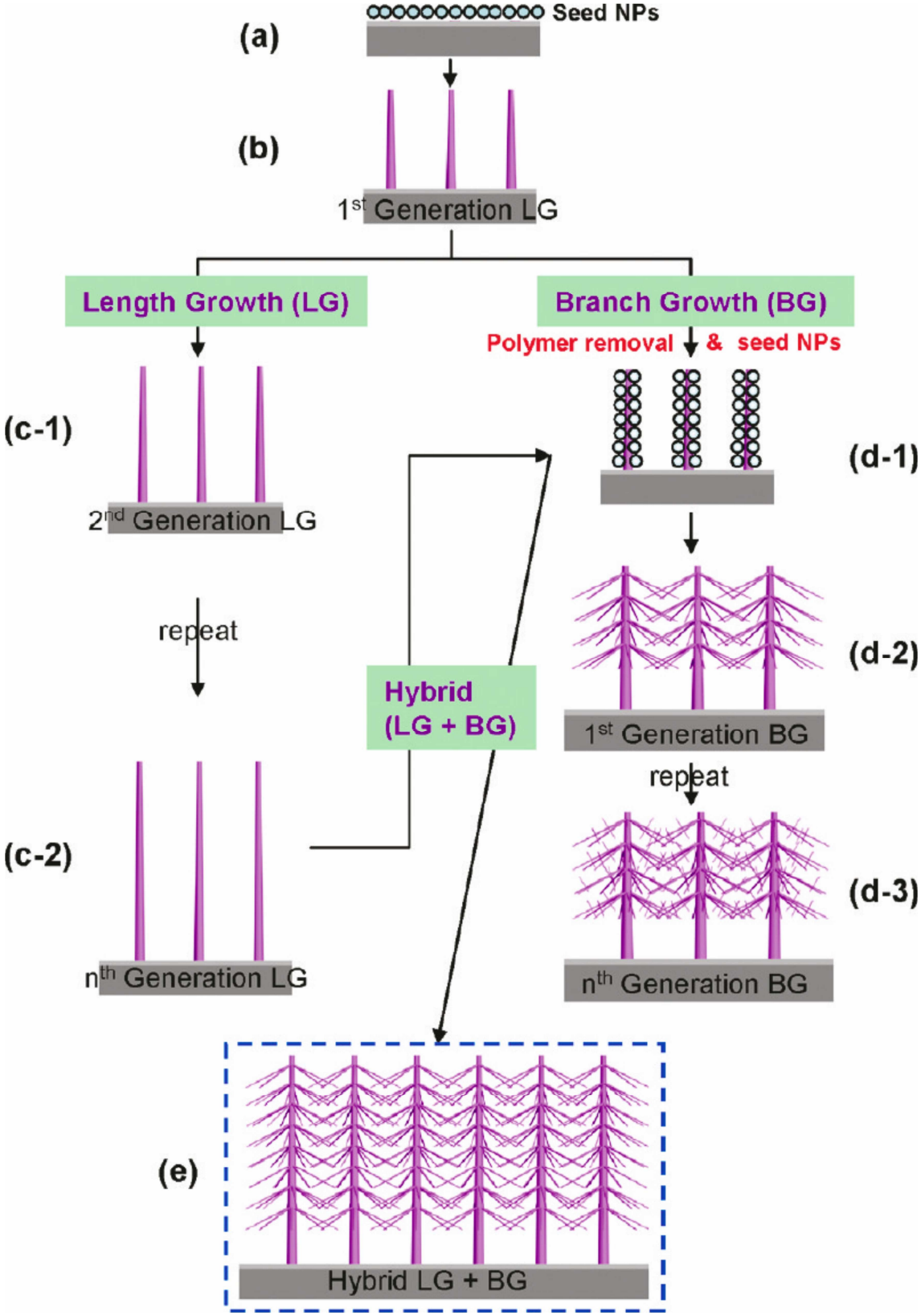

Fig. 8. Two routes for hierarchical ZnO NW hydrothermal growth. Length growth (LG) (a-b-c), branched growth (BG) (a-bd), and hybrid (a-b-c-d-e). Notice polymer removal and seed NPs for branched growth. Reproduced with permission of the *American Chemical Society.*

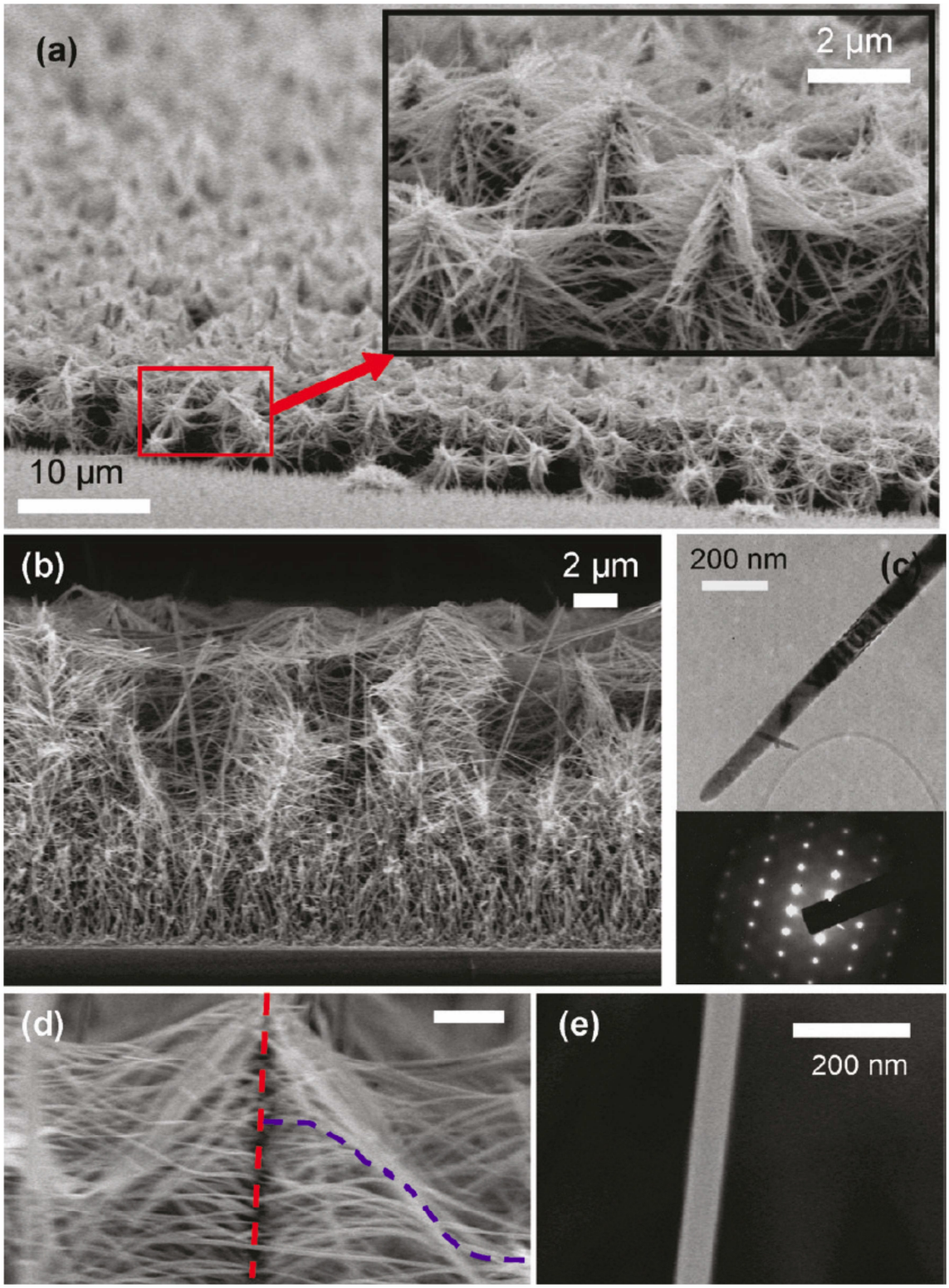

Fig. 9. SEM pictures of ZnO nanowire forest: (a) tilted view, (b) cross section view, (d) magnified view of backbone (red dotted line) and first generation branches (blue dotted line), and (e) magnified view of a branch. (c) TEM picture and selected area electron diffraction pattern of a ZnO nanowire. Reproduced with permission of the *American Chemical Society*.

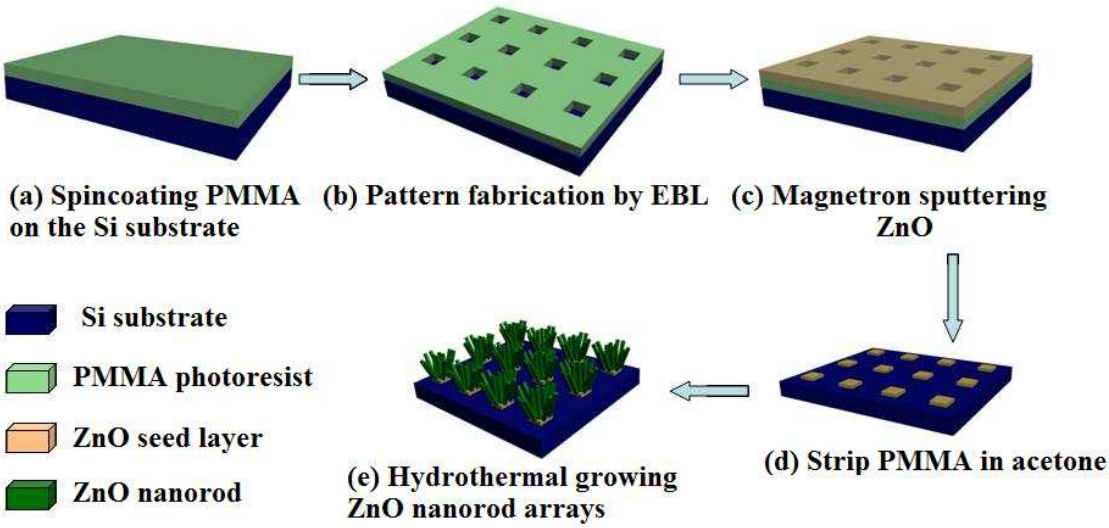

Fig. 10. Schematics of the experimental procedures of patterned ZnO nanorod arrays. (a) Spincoating PMMA on Si substrate; (b) Pattern fabrication by EBL method; (c) Magnetron sputtering ZnO seed layer; (d) Strip PMMA in acetone solution; (e) Hydrothermal growth ZnO nanorods on the patterned areas. Reproduced with permission of the *Springer*.

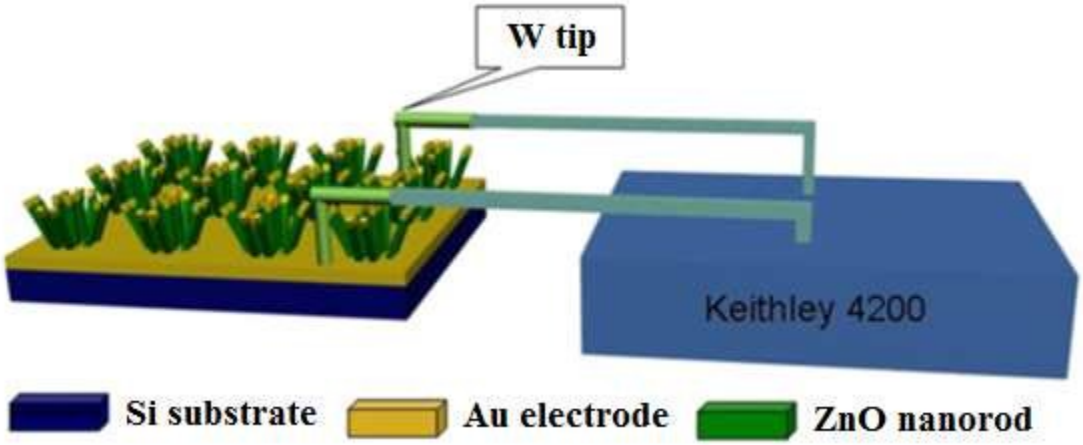

Fig. 11. Schematics of the apparatus used for the synthesis of ZnO nanorod arrays. Reproduced with permission of the *Springer*.

Other methods for ZnO nanoforest fabrication have been also used, although more rarely. Thus, multiple-generation-step deposits of branched ZnO nanostructures were carried out by *vapor phase transport*.[79] The second generation of ZnO nanowires was grown on the first one. Depositing the third generation, the diameter of the branches decreases and the number of branches increases, meanwhile the fourth generation leads to the nanoforest-like morphology. Comparing such branched ZnO forest-like nanostructures with ZnO upstanding nanowire analogues, it was established,[80] that the light-conversion efficiency for dye-sensitized solar cells (DSSC) of the high-density ZnO nanoforest, made of branched ZnO nanowire photoanodes, was found to be about 5 times higher than that of DSSC's comprising of upstanding ZnO nanowires. Applying structural approaches to reach a large increase of the surface area for ZnO nanostructure, ZnO 3D nanostructures ({1011}-stacked nanocones and {1010}-

nanoforest) were fabricated by *facet-selective etching* and *oriented nanocrystal growth*, respectively.[81] In comparison with original ZnO hexagonal nanocone structures, the 3D structures above exhibited a much higher photocatalytic property for photodegradation of Rhodamine *B*. Growth control can be also carried out by other methods. Thus, the control of ZnO nanowire growth with uniform height, diameters, and high crystalline quality was studied by a *focused-ion-beam* (FIB) assisted approach, using an alloy Au-Ga catalyst at 880-940^{o}C.[82] Observing the differences in growth behavior and mechanisms for ZnO nanowires using Au and Au-Ga, it was revealed that, in particular, the FIB-assisted process led to improved nanowire uniformity. In addition, a straightforward method, based on two-photon absorption of a gating photon and a probe photon, was developed to measure the diffusive dwell time of light inside ZnO nanowire forests.[83] It was suggested that the light dwell time can be well predicted from SEM images.

Doped or mixed composite nanoforests of ZnO with other metal oxides are also known. Thus, 3D core/shell ZnO/MnO_2 branched nanowire arrays (Fig. 12), fabricated as it is shown in Fig. 13, exhibited five times larger areal capacitance, smaller inner resistance and better rate performance than their nanowire array counterparts.[84] Electrodes on this 3D nanoforest basis possess considerable application potentials for miniaturized energy storage devices. In addition, *nanosecond pulsed laser deposition* (Figs. 14-15),[85] used for preparation of a forest of Al-doped ZnO nanotrees at high O_2 pressures, can be also applied to fabricate other metal oxides important for technological applications such as Nb_2O_5 (see below), TiO_2, Al_2O_3, WO_3 and Ag_4O_4.

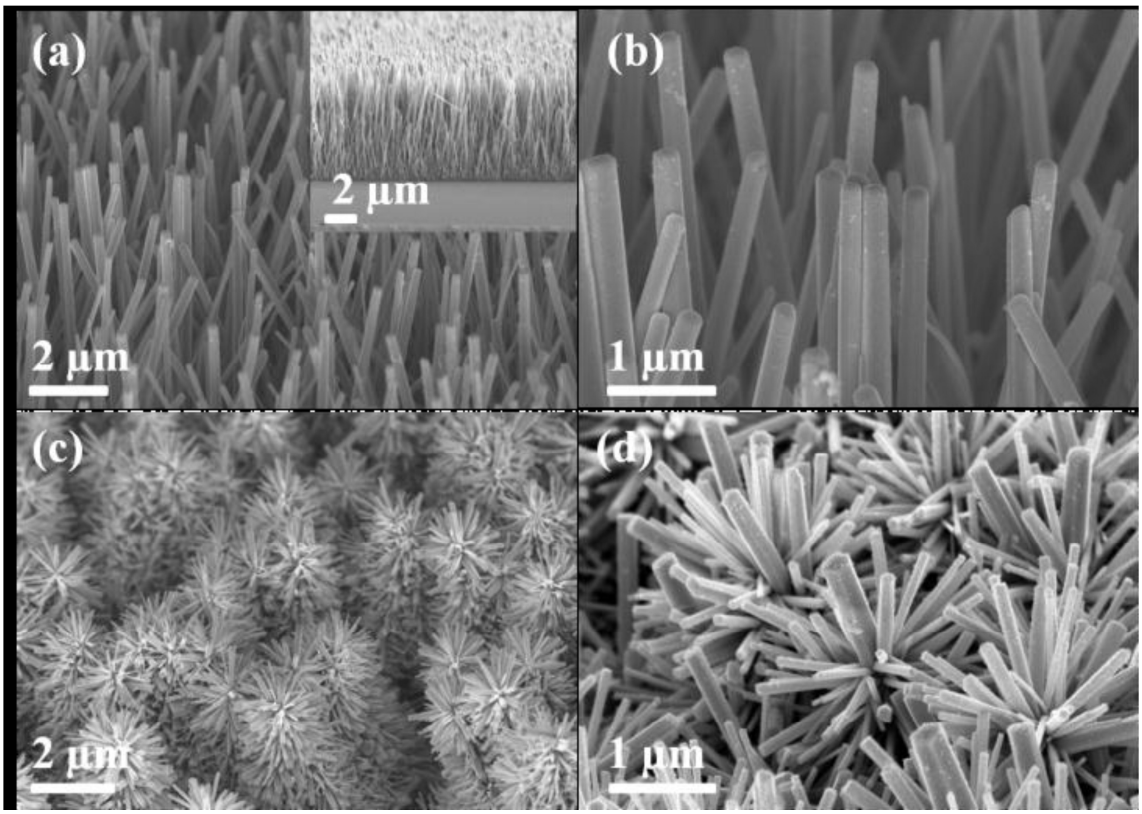

Fig. 12. Typical SEM images of the synthesized 3D ZnO@MnO_2 core@shell (a & b) nanowire arrays and (c, d) forest of nanotrees. Reproduced with permission of the *Royal Society of Chemistry*.

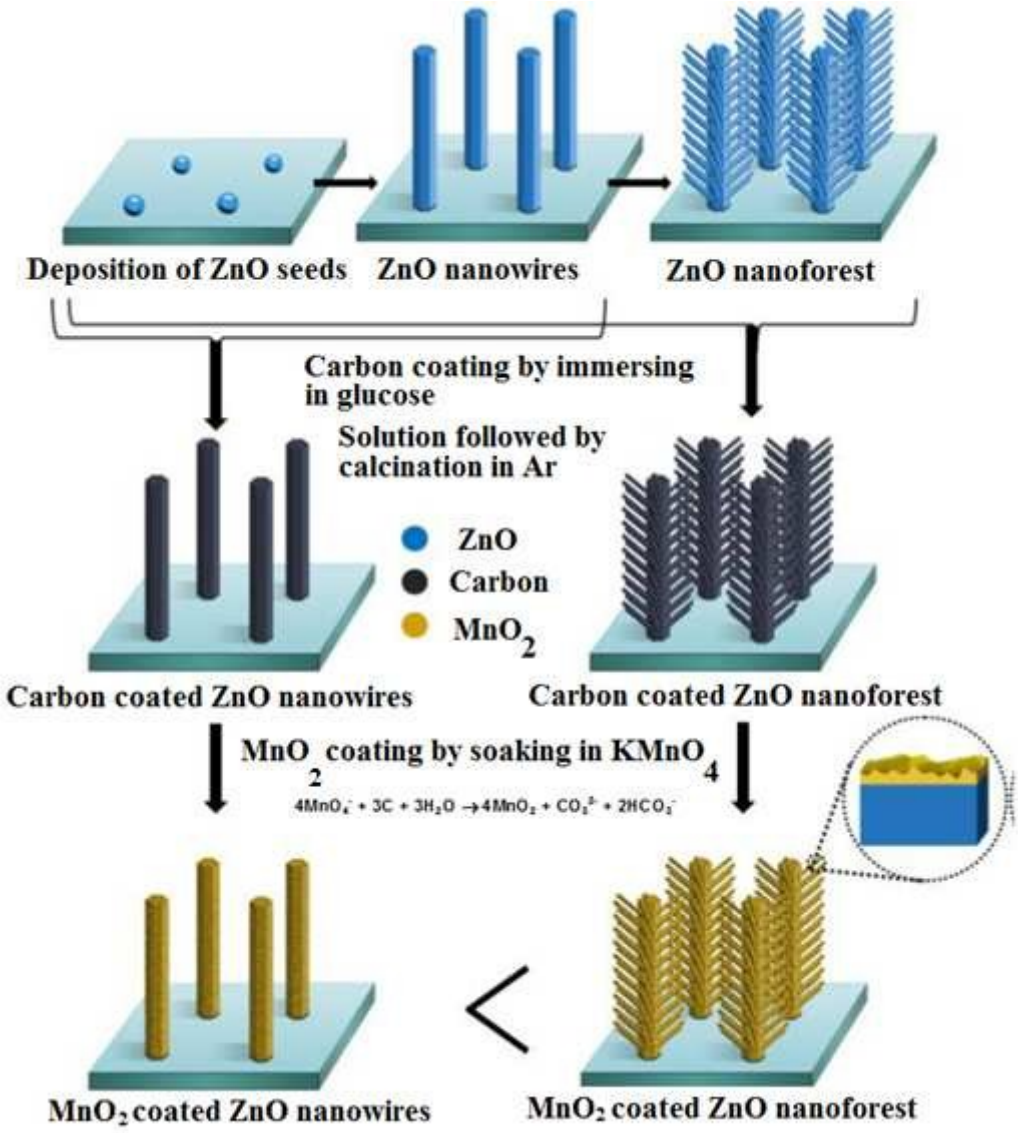

Fig. 13. Schematic illustration of the fabrication process for the designed 3D ZnO/MnO_2 core/shell nanowire array electrode and the nanoforest counterpart. Reproduced with permission of the *Royal Society of Chemistry*.

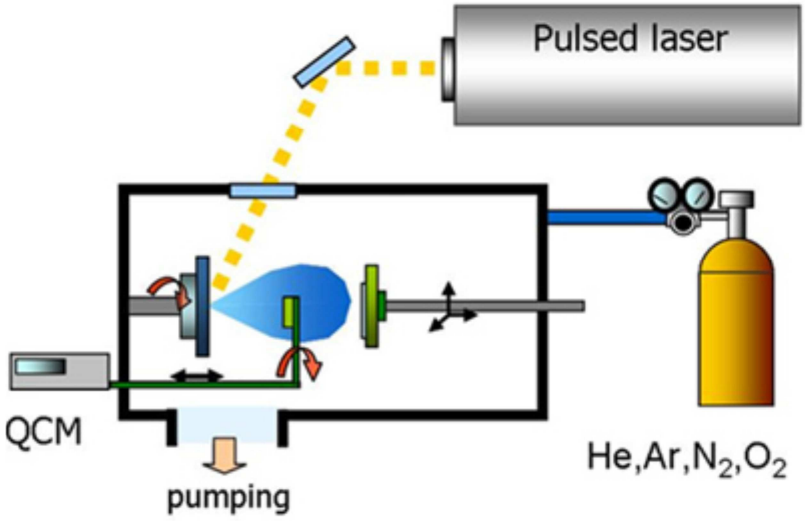

Fig. 14. Scheme of the pulsed laser deposition apparatus. Reproduced with permission from *Journal of Visualized Experiments*.

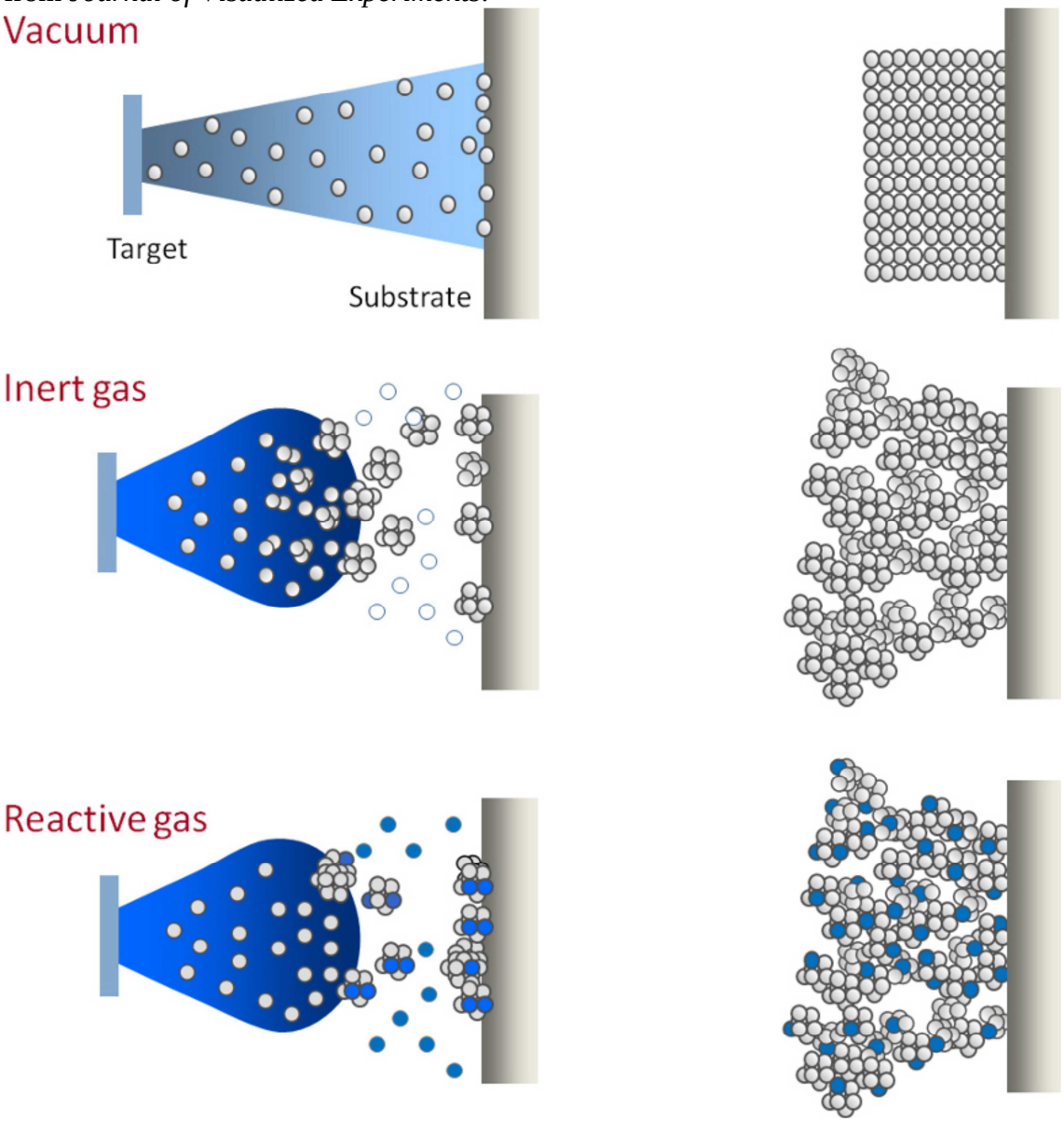

Fig. 15. Pictorial view of the deposition process in vacuum and in the presence of inert and reactive gases. Reproduced with permission from *Journal of Visualized Experiments*.

Silicon nanoforests

Silicon nanowires (SiNW) are known as excellent materials for use in highly-efficient and cost effective thermoelectric devices.[86] These applications were reviewed recently, for instance, the application of electrical SiNW-based devices in the gas phase.[87] The top-down techniques of their production including oxidation, lithography, and anisotropic etching (plasma, wet, and metal-assisted) are well-established.[88] Nanoforests on Si nanowire basis should therefore have much demand and applications in distinct device types.[89 90] Thus, a 3D symmetric micro-supercapacitor was created on the basis of polypyrrole (PPy) coated silicon nanotree (SiNTr) hybrid electrodes was fabricated by a two-step process including Si nanotrees *CVD-assisted growth* on Si substrates and further electrochemical deposit of conducting polymer.[91] Resulting remarkable cycling

stability after thousands of cycles showing a loss of approximately 30% was revealed. Low-reflective "black silicon" surface was produced by a *pulsed deep reactive etching technology* at r.t., varying bias power duty circle and etching window size.[92] At 0.25 duty cycle, the height of the Si forest was found to be to about 10 μm and 0.9% reflectance. Also, nanopillar-forests (heights of several microns, density 20/μm^2, and tip diameters 5-10 nm) with numerous nanoscale gaps were fabricated on the basis of advantage of convexes on Poly-Si surfaces as support structures in sidewall technology.[93] Showing a high SERS-active capability, they may have applications in biological monitoring and chemical detection.

Water splitting continues nowadays to be one of hot topics in the nanotechnology and creation of novel ecomaterials, in particular on silicon basis. Thus, using an artificial photosynthesis system containing an interfacial layer for charge transport, two semiconductor light absorbers with large surface area, and spatially separated cocatalysts to facilitate the water reduction and oxidation, on the basis of Si nanowire array (Fig. 16) a 0.12% solar-to-fuel conversion efficiency was reached: the efficiency of these results is comparable with natural photosynthesis processes.[94]

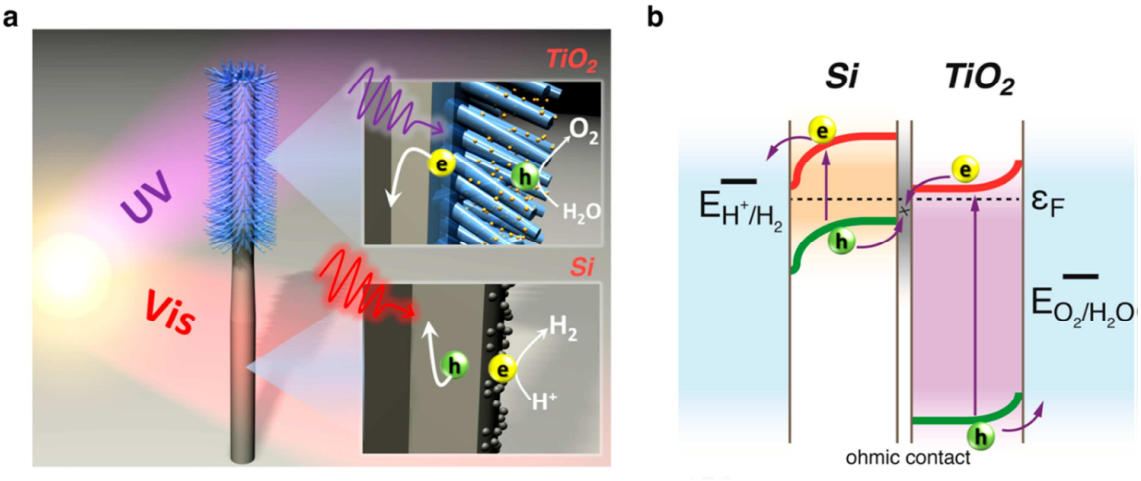

Fig. 16. Schematics of the asymmetric nanoscale tree-like heterostructures used for solar-driven water splitting: a) Structural schematics of the nanotree heterostructure. The small diameter TiO_2 nanowires (blue) were grown on the upper half of a Si nanowire (gray), and the two semiconductors absorb different regions of the solar spectrum. The two insets display the photoexcited electron−hole pairs that are separated at the semiconductor-electrolyte interface to carry out water splitting with the help of cocatalysts (yellow and gray dots on the surface); b) Energy band diagram of the nanotree heterostructure for solar-driven water splitting. The photogenerated electrons in Si and holes in TiO_2 move to the surface to perform water splitting, while the holes in Si and electrons in TiO_2 recombine at the ohmic contact between the two semiconductors. Reproduced with permission of the *American Chemical Society.*

TiO_2 and other transition metal oxides and their hydrated forms

Similarly to ZnO nanoforests described above, titanium dioxide nanoforests are frequently prepared by the hydrothermal synthesis[95] and applied mainly for solar cell purposes as photoanodes with high conversion energy efficiency.[96] Thus, this technique

was applied to obtain TiO_2 hierarchical nanoforest structures without the use of any template or additive (reactions *6-7*).[97] The transformation mechanism "nanorod → nanotree" arrays was proposed and shown in Fig. 17. This type of structures combining the properties of 1D and 3D nanostructures could have more interesting properties than simple arrays of nanorods because of their higher porosity and specific surface area, where the nanobranches with good connections to the trunk. Maximum energy conversion efficiency was observed using DSSCs made of these films containing a thin "adhesive" layer of nanocrystalline TiO_2, for higher dye loading and light harvesting.

$$H_2SO_4 + H_2Ti_2O_5 \cdot H_2O \rightarrow Ti(SO_4)_2 + H_2O \quad (6)$$

$$Ti(SO_4)_2 + H_2O \rightarrow TiO_2 + H_2SO_4 \quad (7)$$

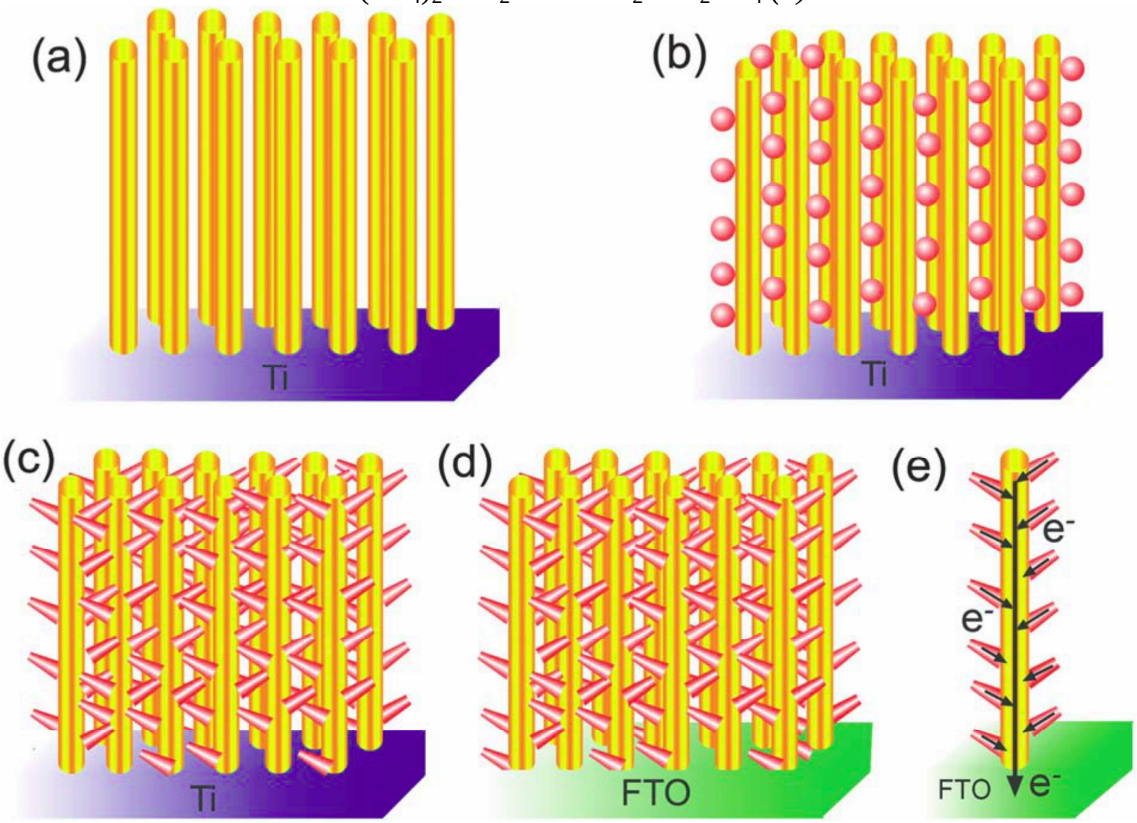

Fig. 17. (a)–(d) Schematic procedure for the formation of the forest-like hierarchical photoanodes. (e) A cartoon of the presumed preferential electron pathway in the hierarchical photoanodes. Reproduced with permission of the *Royal Society of Chemistry.*

Flexible DSSC (reviewed in[98]) belong currently also to an area of elevated interest. Thus, highly efficient Ti substrate-based all-flexible DSSC, containing a TiO_2 nanoforest underlayer (prepared by 3-step process using acid, H_2O_2, and $TiCl_4$ treatment), were prepared.[99] These DSSC showed a relatively high conversion energy efficiency of 8.46%. As an example of other battery anode application, the nanoforests of parallel self-organized sodium titanate/titania nanotrees were obtained by a several-step process including an anodic oxidation of Ti foils to form amorphous TiO_2 nanotubes, sodium insertion, thermal dehydration and crystallization of $Na_2Ti_6O_{13}$/rutile nanotrees.[100] The height (about 8.0 μm) of the nanotubes was found to be similar to the nanoforest, but the morphology varied from aligned nanotubes to complex-texture nanotrees. This material can be applied as high-performance anode for Na-ion microbatteries.

Other transition metal oxides are represented by a few examples, as, for instance Co_3O_4@$NiCo_2O_4$ nanoforests.[101] Single-crystalline β-cobalt hydroxide {β-$Co(OH)_2$} hexagonal-phase nanostructures with distinct morphologies, in particular having a forest-like shape, were hydrothermally prepared in large scale in supercritical water (SCW) and triethylamine (both an alkaline and a complexing reagent) from Co powder (metal source).[102] Varying the ratio "SCW : triethylamine", branched (nanoforest, Fig. 18, ratio 2:1) or non-branched nanowires (ratio 1:0), and nanobelts having branched nanoneedles (ratio 1:2) were obtained.

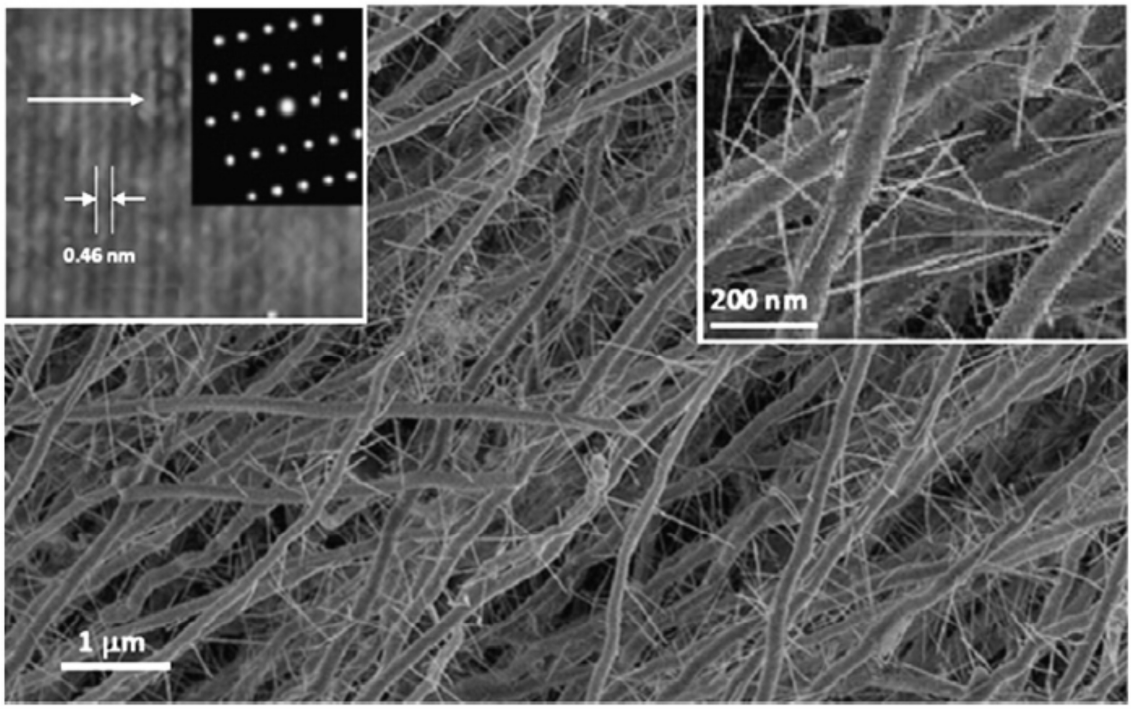

Fig. 18. Images of forest-like cobalt hydroxide structure. Reproduced with permission of the *Elsevier Science.*

Nanoforests of vertically aligned Nb_2O_5 nanocrystals were prepared by *pulsed laser deposition* (see its description above).[103] It was found that a partial pressure of oxygen is needed to develop this growth, revealing the importance of gas composition and pressure. The formed material was tested in DSSC as a photoanode material. Also, a forest structure on the basis of vertically aligned VO_2(B) nanobelt s(NB) was solvothermally prepared using a vertically oriented graphene (VOG) network as the underlying support (Fig. 19).[104] After its further expansion to a 3D folded forest using folded conductive Ni foam (Fig. 20), the final material was tested as electrode for energy storage, showing an excellent performance confirmed by a stable discharge capacity and high cycling stability (>2000 cycles).

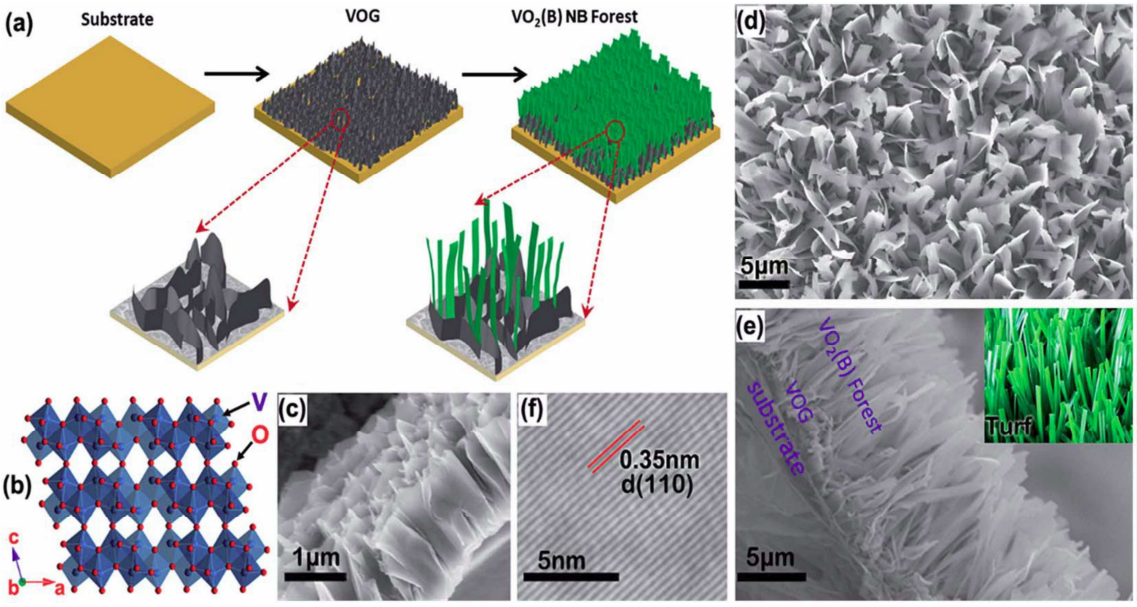

Fig. 19. (a) Schematic showing the synthesis of a VO_2(B) NB-based forest structure on a VOG-coated flat substrate. (b) Lattice structure illustrating the double-layered crystal structure of VO_2(B). Crystal directions a, b and c represent [100], [010], [001] directions, respectively. (c) Cross-sectional SEM image of VOG. (d and e) SEM images of a representative VO_2(B) NB forest with the width of an individual NB of 1–2 mm. The inset of (e) depicts a photo of artificial turf for comparison. (f) High-resolution TEM image indicating the single-crystal structure of an individual NB. The lattice spacing of 0.35 nm corresponds to the (110) crystal plane of VO_2(B). Reproduced with permission of the *Royal Society of Chemistry*.

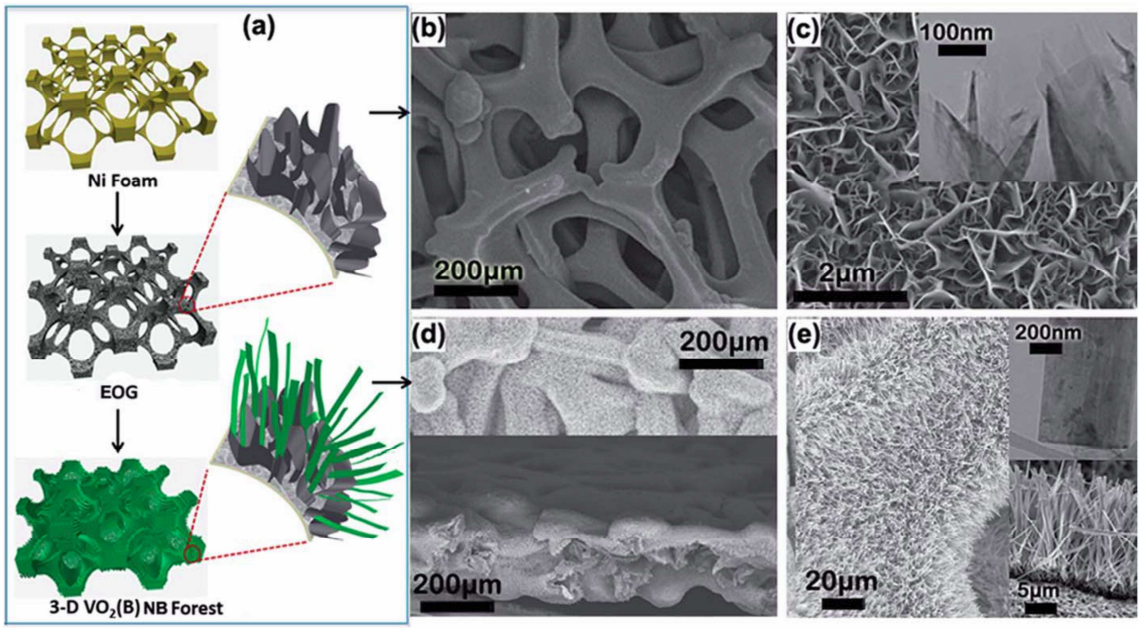

Fig. 20. (a) Schematic of 3D VO_2(B) NB forest synthesis showing that the EOG structure is first grown around the Ni foam skeleton, and then, using the EOG/Ni foam as a support, 3D VO_2(B) NB forest structure is synthesized inside the foam. (b and c) SEM images of the EOG/Ni foam. The inset of (c) is the TEM image of the EOG flake. (d and e) SEM images of the 3D VO_2(B) NB forest. The inset of (d) is the cross-sectional view SEM image of the VO_2(B) NB forest in the EOG/Ni foam that indicates most space in the foam is occupied by the VO_2(B) active material. The top inset of (e) is

the TEM image of an individual NB, and the bottom inset of (e) is the cross-sectional view SEM image of the NB forest. Reproduced with permission of the *Royal Society of Chemistry*.

Mono- and polymetallic nanoforests

Metal-based nanoforests are limited by Au, Sn and some Pt/Ag nanostructures. Thus, highly unconventional anisotropic growth of forest made of gold nanowires from nanocrystals was recently discussed.[105] In particular, a) nanowires cannot grow from colloidal seeds, but they can grow from substrate-bound seeds, b) nanowires can grow from only one side of the seeds, and their diameter is independent on seeds size, c) ultrathin, vertically aligned nanowires were observed on substrates with use of aqueous solution at r.t. It was suggested that, in this system, the strong binding of ligands leads to selective deposition of gold at the ligand-deficient interface between Au seeds and oxide substrates (Fig. 21). Gold nanoforests can have certain applications. Thus, densely packed Au nanowires were vertically grown on 3-aminopropyltriethoxy silane functionalized glass slides[106] and used as a sensor for the multiple detection of malachite green, 1-naphthalenethiol and rhodamine 6G in aqueous solution (detection limit 10^6 m). A complex 3D nanoforest on the basis of Sn nanorods having a core-shell structure was grown on genetically engineered viral scaffolds.[107] The resulting material exhibited supreme capacity utilization and cycling stability toward Na-ion storage and release.

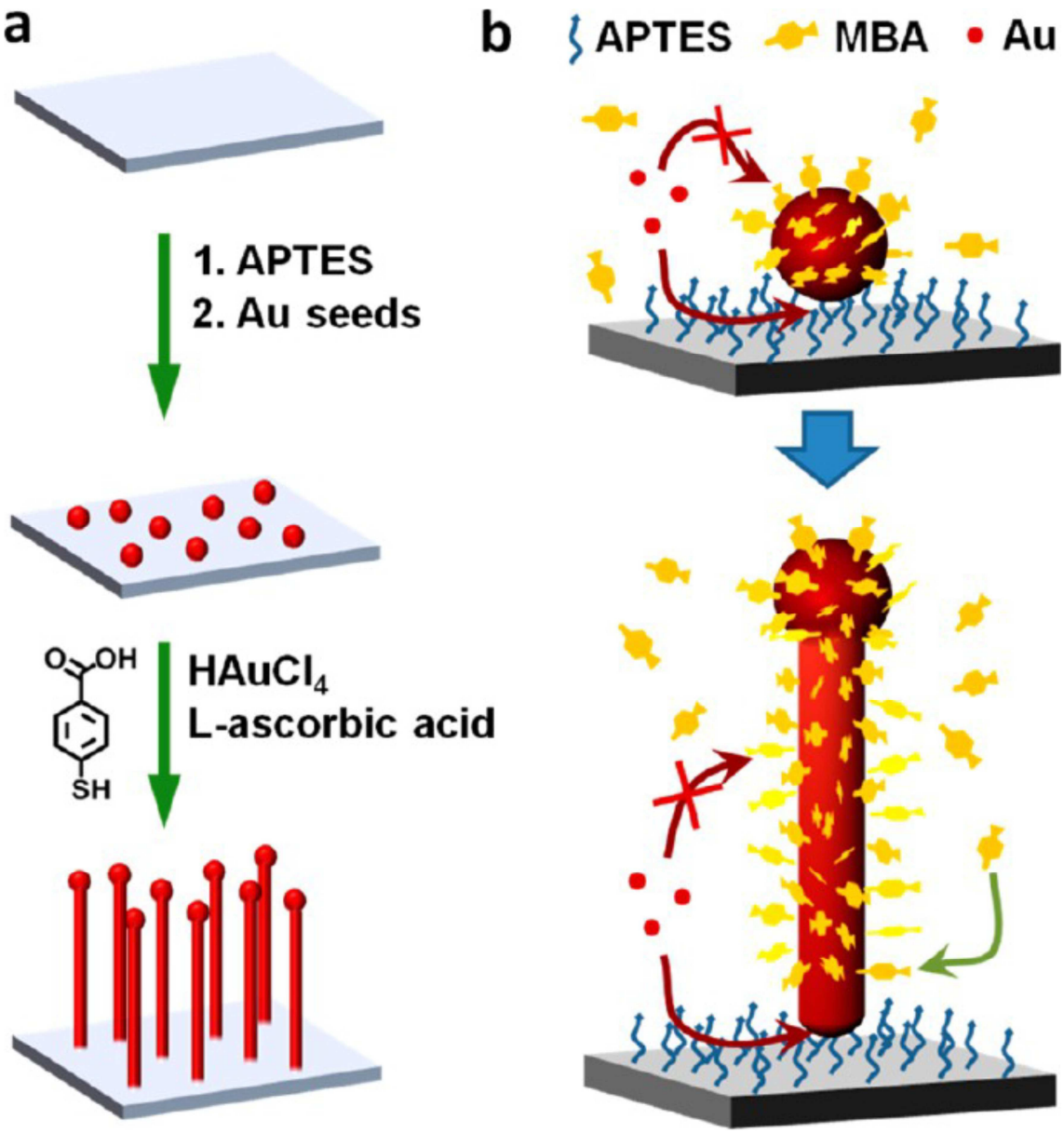

Fig. 21. (a,b) Schematics illustrating (a) the specific conditions used for the syntheses of AuNWs on Si/SiO_2 substrates; (b) because of the strong ligands, the Au deposition selectively occur at the Au substrate interface. Reproduced with permission of the *American Chemical Society.*

Pt-Ag tubular dendritic nano-forests (tDNFs) were grown by two-step galvanic replacement reaction (Fig. 22) at r.t. and applied for cost-effective methanol oxidation reaction under solar irradiation.[108] The first step was the growth of Ag nanoforests (10 μm in thickness) on silicon wafer in $AgNO_3$ solution and then H_2PtCl_6 was used as the precursor for Pt deposition, converting silver dentritic nanoforects into Pt-Ag tDNFs. The observed solar response (6.4% of enhancement on oxidation current) was attributed to the strong LSPR due to the Ag DNFs, so this material can be used in photo-electro-chemical fuel cells. In addition, the nanodendrite forest-like trimetallic structures composed of Pt, Au, and Ag showed an excellent methanol oxidation reaction catalytic activity in comparison with bare Pt electrodes due to larger active surface area.[109]

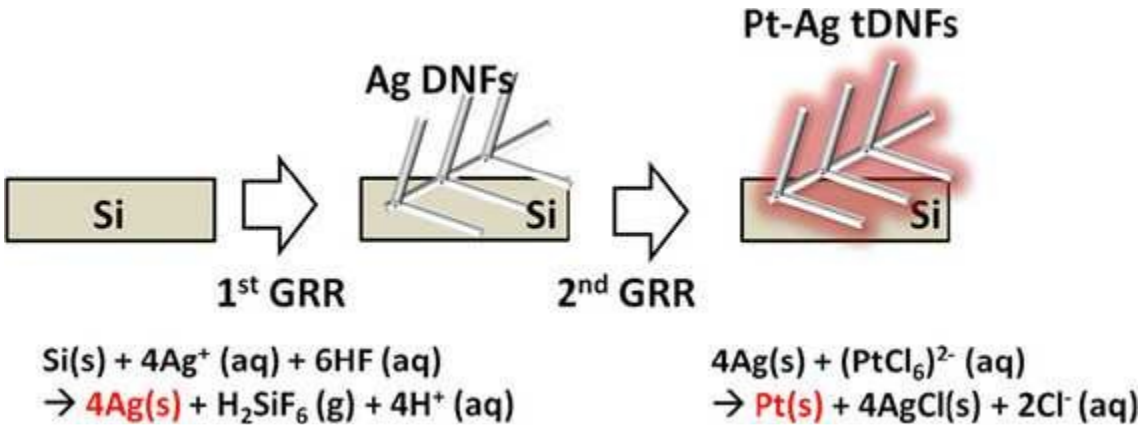

Fig. 22. The schematic drawing of the two-step GRR process. Reproduced with permission of the *Springer*.

Ga/P and Ga/As nanoforests

These nanoforests can be applied for distinct uses, in particular, as supports for biomolecules. Thus, for supported fluorescently labeled phospholipid bilayers, used as a model for biomembranes, the formation of fluid supported bilayers on GaP vertical nanowire forests was observed under self-assembly from vesicles in solution.[110] Another application was reported[111] in the area of functional optical devices, which were fabricated on the basis of GaAs/AlGaAs nanowire forest by sectioning quantum-dot-in-nanowires systems by a “nanoskiving” process (Fig. 23). The quantum dots inside the nanowires are functional exhibiting a photoluminescent emission (wavelengths 650−710 nm).

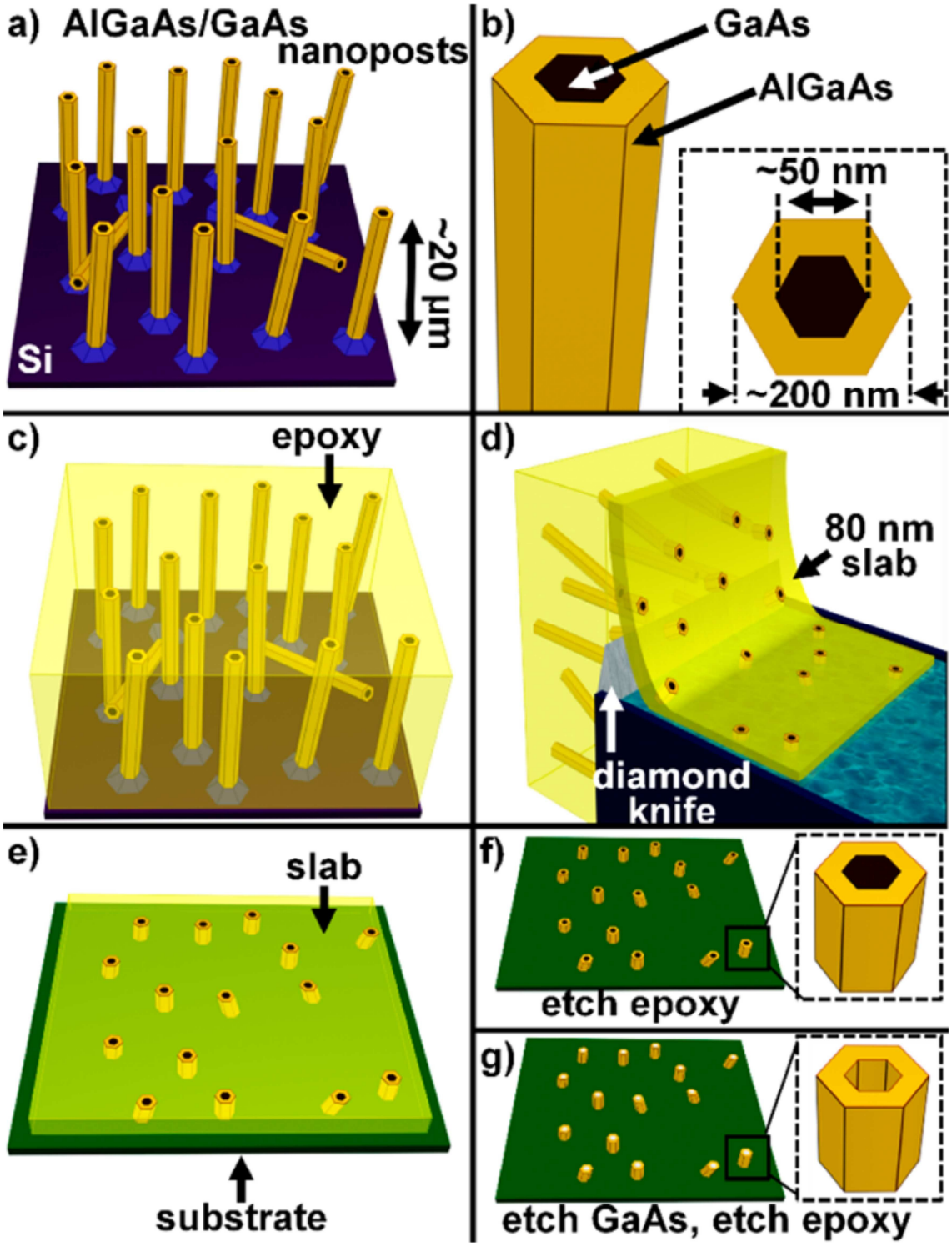

Fig. 23. Nanoskiving process. (a) The GaAs/AlGaAs nanowire forest is grown by MBE on a silicon wafer. (b) The wires are hexagonal with a GaAs core and $Al_{0.75}Ga_{0.25}As$ shell. (c) The nanowire forest is embedded in epoxy and UV-cured. (d) The block of epoxy with the embedded nanowires is then cleaved off and sliced on an ultramicrotome with a diamond blade. (e) The slices are transferred on a new substrate. (f) Optionally, the epoxy can be etched by oxygen plasma, leaving the slices freestanding on the wafer. (g) The core can also be etched by citric acid, leaving hollow-core slices. Reproduced with permission of the *American Chemical Society*.

Organic nanoforests

Nanoforests on the basis of organic compounds are very rare and mentioned in reviews[112 113] and are made mainly of peptides, for example diphenylalanine.[114] Thus, peptide nanoforest (Fig. 24) biosensors, tested for phenol detection, were found to be more sensitive than those modified with carbon nanotubes or combined coating and 17-fold more sensitive than uncoated electrode.[115] Several applications for organic nanoforests, for instance for tobacco mosaic virus nanoforest arrays, were achieved for preparation of 3D patterned $LiFePO_4$ nanorods, used in lithium batteries.[116]

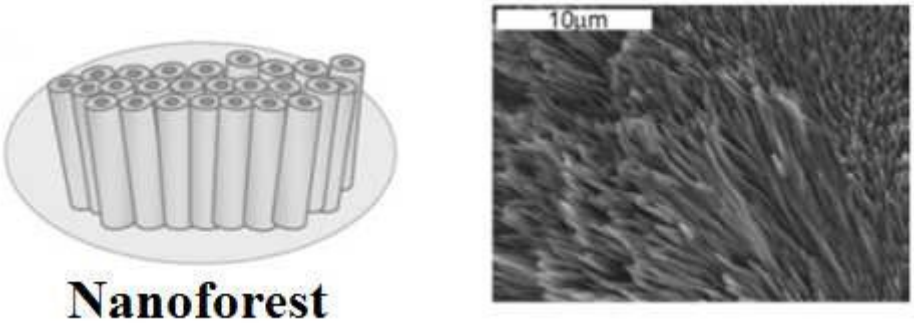

Fig. 24. FF (diphenylalanine) peptide nanoforest deposited on an electrode, illustration and SEM image, respectively. Reproduced with permission of the *John Wiley & Sons.*

Conclusions

Nano- and micrometric forest-like structures are generally made of more simple 1D nanostructures, such as nanowires, nanopillars, nanorods, nanotrees, nanofibers or nanotubes. They are generally known for simple inorganic compounds and well-studied mainly for carbon nanotubes and zinc oxide. In case of CNTs, their nanoforests are currently known as the darkest artificially produced materials. For different compounds, synthesis methods can vary. If for CNT nanoforests main methods are CVD / spray pyrolysis / thermal decomposition of such hydrocarbons as C_2H_2, where the nanoforest grows on metal catalysts, or electrophoretic deposition, for ZnO nanoforests the principal method is hydrothermal route, among other methods, such as electron beam lithography (as well as lithography-free approach[117]), focused-ion-beam technique, vapor phase transport, facet-selective etching and oriented nanocrystal growth. For the formation of silicon nanoforests, pulsed deep reactive etching technology and pulsed laser deposition are preferable.

Nowadays, the nanoforests possess a variety of applications, for instance as sensors / detectors for glucose, phenol, malachite green, 1-naphthalenethiol, rhodamine 6G, among others (CNTs, Au, organic nanoforests), photoanodes in solar[118] and fuel cells with high photoconversion efficiency, supercapacitors and energy storage devices (ZnO, Pt-Ag, Si, TiO_2), SERS applications (CNTs, Si), optical and MEMs switching devices (CNTs, GaAs/AlGaAs), as well as for water splitting processes (Si), CO_2 fixation,[119] and as supports for biomolecules (GaP). The vertical nanowires can be applied to study proteins (target of a range of different drugs), which are active in the cell membranes, so the nanoforest could be of great importance both for pharmaceutical research as basic cell research.[120] One of causes for their advantages is that nanoforests have shown much larger surface area in comparison with non-branched / upstanding nanowires and

nanorods. As a concluding remark, forest-like nanostructures are currently actively studied[121 122] and it is expected that more varieties of compounds can be obtained in this form and find useful applications.

References

[1] Y. B. Zhang, S.P. Lau, H. F. Li, Field emission from nanoforest carbon nanotubes grown on cobalt-containing amorphous carbon composite films, *Journal of Applied Physics*, 2007, **101**(3), 033524/1–033524/5.

[2] C.-H. Xue, R.-L. Wang, J. Zhang, S.-T. Jia, L.-Q. Tian, Growth of ZnO nanorod forests and characterization of ZnO-coated nylon fibers, *Materials Letters*, 2010, **64**(3), 327–330.

[3] F. M. B. Hassan, H. Nanjo, S. Venkatachalam, M. Kanakubo, T. Ebina, Effect of the solvent on growth of titania nanotubes prepared by anodization of Ti in HCl, *Electrochimica Acta*, 2010, **55**(9), 3130–3137.

[4] M. Reches, E. Gazit, Controlled patterning of aligned self-assembled peptide nanotubes. *Nature Nanotechnology*, 2006, **1**(3), 195–200.

[5] M. Wanit, J.b Yeo, S. J. Hong, Y. D. Suh, S. Hwan Ko, D. Lee, C. P. Grigoropoulos, ZnO nano-tree growth study for high efficiency solar cell, *Energy Procedia*, 2012, **14**, 1093–1098.

[6] J. W. Yancey, Solderless carbon nanotube and nanowire electrical contacts and methods of use thereof, US Patent 2011/0039459, 2011.

[7] S. Guha, O. Gunawan, Photovoltaic devices with enhanced efficiencies using high-aspect-ratio nanostructures. US Patent 8592675 B2, 2013.

[8] G. Pennelli, Review of nanostructured devices for thermoelectric applications, *Beilstein J. Nanotechnol*., 2014, **5**, 1268–1284.

[9] J.N. Tiwari, F.-M. Pan, K.-L. Lin. Facile approach to the synthesis of 3D platinum nanoflowers and their electrochemical characteristics. *New Journal of Chemistry*, 2009, **33** (7), 1482-1485.

[10] J.N. Tiwari, R.N. Tiwari, K.-L. Lin. Controlled Synthesis and Growth of Perfect Platinum Nanocubes Using a Pair of Low-Resistivity Fastened Silicon Wafers and Their Electrocatalytic Properties. *Nano Research*, 2011, **4** (6), 541-549.

[11] J.N. Tiwari, F.-M. Pan, T.-M. Chen, R.N. Tiwari, K.-L. Lin. Electrocatalytic activity of Pt nanoparticles electrodeposited on amorphous carbon-coated silicon nanocones. *Journal of Power Sources*, 2010, **195** (3), 729-735.

[12] J.N. Tiwari, K. Christian Kemp, K. Nath, R.N. Tiwari, H.-G. Nam, K.S. Kim. Interconnected Pt-Nanodendrite/DNA/Reduced-Graphene-Oxide Hybrid Showing Remarkable Oxygen Reduction Activity and Stability. *ACS Nano*, 2013, **7** (10), 9223–9231.

[13] J.N. Tiwari, K. Nath, S. Kumar, R.N. Tiwari, K. Christian Kemp, N.H. Le, D. H. Youn, J. S. Lee, K.S. Kim. Stable platinum nanoclusters on genomic DNA–graphene oxide with a high oxygen reduction reaction activity. *Nature Communications*, 2013, **4**, 2221.

[14] J.N. Tiwari, R.N.Tiwari, G. Singh, K.S. Kim. Recent progress in the development of anode and cathode catalysts for direct methanol fuel cells. *Nano Energy*, 2013, **2** (5), 553–578.

[15] J.N. Tiwari, F.-M. Pan, R. N. Tiwari , S.K. Nandi. Facile synthesis of continuous Pt island networks and their electrochemical properties for methanol electrooxidation. *Chemical Communications*, 2008, 6516-6518.

[16] J.N. Tiwari, R.N. Tiwari, K.-L. Lin. Synthesis of Pt Nanopetals on Highly Ordered Silicon Nanocones for Enhanced Methanol Electrooxidation Activity. *ACS Applied Mat. Interfac.*, 2010, **2** (8), 2231-2237.
[17] J.N. Tiwari, R.N. Tiwari, Y.-M. Chang, K.-L. Lin. A Promising Approach to the Synthesis of 3D Nanoporous Graphitic Carbon as a Unique Electrocatalyst Support for Methanol Oxidation. *ChemSusChem*, 2010, **3** (4), 460-466.
[18] Y. Yoon, D. Kim, J.-B. Lee. Hierarchical micro/nano structures for super-hydrophobic surfaces and super-lyophobic surface against liquid metal. *Micro and Nano Systems Letters*, 2014, **2**:3. http://link.springer.com/article/10.1186%2Fs40486-014-0003-x#
[19] J. N. Tiwari, R. N. Tiwari, K. S. Kim. Zero-dimensional, one-dimensional, two-dimensional and three-dimensional nanostructured materials for advanced electrochemical energy devices. *Progress in Materials Science*, 2012, **57**, 724–803.
[20] H. Butt, R. Rajesekharan, Q. Dai, S. Sarfraz, V. Kumar R., G .A. J. Amaratunga, T. D. Wilkinson, Cylindrical Fresnel lenses based on carbon nanotube forests, *Applied Physics Letters*, 2012, **101**(24), Article number 243116.
[21] T. Saleh, M. Vahdani Moghaddam, M. Sultan Mohamed Ali, M. Dahmardeh, C. Alden Foell, A. Nojeh, K. Takahata Transforming carbon nanotube forest from darkest absorber to reflective mirror, *Appl. Phys. Lett*., 2012, **101**, 061913.
[22] H. Chen, A. Roy, J.-B. Baek, L. Zhu, J. Qu, L. Dai, Controlled growth and modification of vertically-aligned carbon nanotubes for multifunctional applications, *Mater. Sci. Eng. R: Reports*, 2010, **70**, 63-91.
[23] N. Hayashi, S.-I. Honda, K. Tsui, K.-Y. Lee, T. Ikuno, K. Fujimoto, S. Ohkura, M. Katayama, K. Oura, T. Hirao. Highly aligned carbon nanotube arrays fabricated by bias sputtering, *Appl. Surf. Sci*. 2003, 212-213 393-396.
[24] C. Daraio, V. F. Nesterenko, S. Jin, Impact response by a foamlike forest of coiled carbon nanotubes, *J. Appl. Phys*. 2006, **100**, 064309, 4 pp..
[25] Y. Taki, M. Kikuchi, K. Shinohara, A. Tanaka, Selective Growth of Vertically Aligned Single-, Double-, and Triple-Walled Carbon Nanotubes by Radiation-Heated Chemical Vapor Deposition, *Jpn. J. Appl. Phys*. 2008, **47**, 721-724.
[26] A. M. Cassell, M. Meyyappan, J. Han, Multilayer Film Assembly of Carbon Nanotubes, *J. Nanopart. Res*. 2000, **2**(4), 387-389.
[27] Q. Zhang, W. Zhou,W. Qian, R. Xiang, J. Huang, D. Wang, F. Wei, Synchronous Growth of Vertically Aligned Carbon Nanotubes with Pristine Stress in the Heterogeneous Catalysis Process, *J. Phys. Chem. C*, 2007, **111**, 14638-14643.
[28] X. Li, A. Cao, Y. J. Jung, R. Vajtai, P. M. Ajayan, Bottom-Up Growth of Carbon Nanotube Multilayers: Unprecedented Growth, *Nano Lett*. 2005, **5**, 1997-2000.
[29] S. Huang, L. Dai, A. W. H. Mau, Nanotube “crop circles”, *J. Mater. Chem*. 1999, **9**, 1221-1222.
[30] C. K. Tan, K. P. Loh, T. T. L. John, Direct amperometric detection of glucose on a multiple-branching carbon nanotube forest, *Analyst*, 2008, **133**, 448-451.
[31] S. Li, H. Li, X. Wang, Y. Song, Y. Liu, L. Jiang, D. Zhu, Super-Hydrophobicity of Large-Area Honeycomb-Like Aligned Carbon Nanotubes, *J. Phys. Chem. B*, 2002, **106**(36) 9274-9276.
[32] M. R. Maschmann, Integrated simulation of active carbon nanotube forest growth and mechanical compression, *Carbon*, 2015, **86**, 26-37.
[33] E. G. Rakov, Materials made of carbon nanotubes. The carbon nanotube forest. *Russian Chemical Reviews*, 2013, **82**(6), 538-566.

[34] M. Pinault, V. Pichot, H. Khodja, P. Launois, C. Reynaud, M. Mayne-L'Hermite, Evidence of Sequential Lift in Growth of Aligned Multiwalled Carbon Nanotube Multilayers, *Nano Lett.*, 2005, **5**(12), 2394-2398.
[35] R. Xiang, G. Luo, Z. Yang, Q. Zhang, W. Qian, F. Wei, Temperature effect on the substrate selectivity of carbon nanotube growth in floating chemical vapor deposition, *Nanotechnology*, 2007, **18**(41), 415703.
[36] Z. Yang, H. Nie, X. Zhou, Z. Yao, S. Huang, X. Chen, Synthesizing a well-aligned carbon nanotube forest with high quality via the nebulized spray pyrolysis method by optimizing ultrasonic frequency, *Nano*, 2011, **6**, 343-348.
[37] C. Du, N. Pan, High power density supercapacitor electrodes of carbon nanotube films by electrophoretic deposition, *Nanotechnology*, 2006, **17**(21), 5314-5318.
[38] S. Shekhar, P. Stokes, Sl. Khondaker, Ultrahigh Density Alignment of Carbon Nanotube Arrays by Dielectrophoresis, *ACS Nano*, 2011, **5**(3), 1739–1746.
[39] P. Diao, Z. Li, Vertically Aligned Single-Walled Carbon Nanotubes by Chemical Assembly – Methodology, Properties, and Applications, *Adv. Mater*., 2010, **22**, 1430-1449.
[40] C. Soldano, S. Talapatra, S. Kar, Carbon Nanotubes and Graphene Nanoribbons: Potentials for Nanoscale Electrical Interconnects. *Electronics*, 2013, **2**, 280-314.
[41] J. Prasek, J. Drbohlavova, J. Chomoucka, J. Hubalek, O. Jasek, V. Adam, R. Kizek, Methods for carbon nanotubes synthesis—review. *J. Mater. Chem.*, 2011, **21**, 15872–15884.
[42] E. R. Meshot, D. L. Plata, S. Tawfick, Y. Zhang, E. A. Verploegen, A. J. Hart, Engineering Vertically Aligned Carbon Nanotube Growth by Decoupled Thermal Treatment of Precursor and Catalyst. *ACS Nano*, 2009, **3** (9), 2477-2486.
[43] K. Hasegawa, S. Noda, H. Sugime, K. Kakehi, S. Maruyama, Y. Yamaguchi, Growth window and possible mechanism of millimeter-thick single-walled carbon nanotube forests. *Journal of Nanoscience and Nanotechnology*, 2008, **8** (11), 6123-6128.
[44] J. Olivares, T. Mirea, B. Díaz-Durán, M. Clement, M. De Miguel-Ramos, J. Sangrador, J. De Frutos, E. Iborra, Growth of carbon nanotube forests on metallic thin films, *Carbon*, 2015, **90**, 9-15.
[45] H. Sugime, S. Esconjauregui, L. D'Arsié, J. Yang, A. W. Robertson, R. A. Oliver, S. Bhardwaj, C. Cepek, J. Robertson, Low-Temperature Growth of Carbon Nanotube Forests Consisting of Tubes with Narrow Inner Spacing Using Co/Al/Mo Catalyst on Conductive Supports, *ACS Applied Materials and Interfaces*, 2015, **7**(30), 16819-16827.
[46] T. Ohashi, T. Shima, Synthesis of vertically aligned single-walled carbon nanotubes with metallic chirality through facet control of catalysts, *Carbon*, 2016, **87**(1), 453-461.
[47] S. Esconjauregui, M. Fouquet, B. C. Bayer, S. Eslava, S. Khachadorian, S. Hofmann, J. Robertson. Manipulation of the catalyst-support interactions for inducing nanotube forest growth. *J. Appl. Phys*., 2011, **109**, 044303.
[48] Wirth, C. T.; Zhang, C.; Zhong, G.; Hofmann, S.; Robertson, J. Diffusion- and Reaction-Limited Growth of Carbon Nanotube Forests. *ACS Nano*, **2009**, *3* (11), 3560-3566.
[49] M. Bedewy, E. R. Meshot, H. Guo, E. A. Verploegen, W. Lu, A. J. Hart, Collective Mechanism for the Evolution and Self-Termination of Vertically Aligned Carbon Nanotube Growth. *Journal of Physical Chemistry C*, 2009, **113**(48), 20576-20582.
[50] R. Siddheswaran, D. Manikandan, R. E. Avila, C. E. Jeyanthi, R. V. Mangalaraja, Formation of carbon nanotube forest over spin-coated Fe2O 3 reduced thin-film by

chemical vapor deposition. *Fullerenes, Nanotubes and Carbon Nanostructures*, 2015, **23**(5), 392-398.
[51] J. Yang, S. Esconjauregui, A. W. Robertson, Y. Guo, T. Hallam, H. Sugime, G. Zhong, G. S. Duesberg, J. Robertson, Growth of high-density carbon nanotube forests on conductive TiSiN supports, *Applied Physics Letters*, 2015, **106**(8), Article number 083108.
[52] N. Matsumoto, A. Oshima, S. Sakurai, T. Yamada, M. Yumura, K. Hata, D. N. Futaba, The Application of Gas Dwell Time Control for Rapid Single Wall Carbon Nanotube Forest Synthesis to Acetylene Feedstock, *Nanomaterials*, 2015, **5**, 1200-1210.
[53] J. Huang, Q. Zhang, M. Zhao, F. Wei, Process Intensification by CO_2 for High Quality Carbon Nanotube Forest Growth: Double-Walled Carbon Nanotube Convexity or Single-Walled Carbon Nanotube Bowls? *Nano Res*. 2009, **2**, 872-881.
[54] M. Zhang, O. O. I. Okoli, H. Hoang Van, Graphene nanoribbons and methods. US Patent 2015/0013896 A1, 2015.
[55] S. Santhanagopalan, A. Balram, E. Lucas, F. Marcano, D. Desheng Meng, High Voltage Electrophoretic Deposition of Aligned Nanoforests for Scalable Nanomanufacturing of Electrochemical Energy Storage Devices, *Key Engineering Materials*, 2012, **507**, 67-72.
[56] D. S. Jensen, S. S. Kanyal, N. Madaan, M. A. Vail, A. E. Dadson, M. H. Engelhard, M. R. Linford, Multiwalled Carbon Nanotube Forest Grown via Chemical Vapor Deposition from Iron Catalyst Nanoparticles, by XPS. *Surface Science Spectra*, 2013, **20**, 62-67.
[57] G. Chen, Y. Seki, H. Kimura, S. Sakurai, M. Yumura, K. Hata, D. N. Futaba. Diameter control of single-walled carbon nanotube forests from 1.3–3.0 nm by arc plasma deposition. *Sci. Rep*., 2014, **4**, 3804.
[58] M. Vahdani Moghaddam, P. Yaghoobi, G. A. Sawatzky, A. Nojeh. Photon-Impenetrable, Electron-Permeable: The Carbon Nanotube Forest as a Medium for Multiphoton Thermal-Photoemission, *ACS Nano*, 2015, **9**(4), 4064–4069.
[59] N. J. Ginga, W. Chen, S. K. Sitaraman, Waviness reduces effective modulus of carbon nanotube forests by several orders of magnitude, *Carbon*, 2014, **66**, 57–66.
[60] J.-W. Jiang. Strain Engineering for Thermal Conductivity of Single-Walled Carbon Nanotube Forests, Cornell University Library, arXiv:1406.4559.
[61] P. Pour Shahid Saeed Abadi, S. B. Hutchens, J. R. Greer, B. A. Cola, S. Graham, Buckling-driven delamination of carbon nanotube forests, *Appl. Phys. Lett*., 2013, **102**, 223103.
[62] G. Chen, D. N. Futaba, H. Kimura, S. Sakurai, M. Yumura, K. Hata, Absence of an Ideal Single-Walled Carbon Nanotube Forest Structure for Thermal and Electrical Conductivities. *ACS Nano*, 2013, **7**(11), 10218–10224.
[63] P. Joseph, C. Cottin-Bizonne, J.-M. Benoıt, C. Ybert, C. Journet, P. Tabeling, L. Bocquet, Slippage of water past superhydrophobic carbon nanotube forests in microchannels, *Phys. Rev. Lett*., 2006, **97**, 156104.
[64] K. K. S. Lau, J. Bico, K. B. K. Teo, M. Chhowalla, G. A. J. Amaratunga, W. I. Milne, G. H. McKinley, K. K. Gleason. Superhydrophobic Carbon Nanotube Forests. *Nano Letters*, 2003, **3**(12), 1701–1705.
[65] R. Kant, M. Birla Singh, Generalization of the Gouy-Chapman-Stern model of an electric double layer for a morphologically complex electrode: Deterministic and stochastic morphologies. *Phys. Rev. E*, 2013, **88**, 052303.

[66] A. Ozhan Altun, S. Ki Youn, N. Yazdani, T. Bond, H. Gyu Park. Metal-Dielectric-CNT Nanowires for Femtomolar Chemical Detection by Surface Enhanced Raman Spectroscopy. *Adv. Mater*. 2013, **25**(32), 4377-4377.
[67] S. Deng, M. Kurttepeli, D. J. Cott, S. Bals, C. Detavernier, Porous nanostructured metal oxides synthesized through atomic layer deposition on a carbonaceous template followed by calcination, *Journal of Materials Chemistry A*, 2015, **3**(6), 2642-2649.
[68] M. P. Down, A. P. Lewis, L. Jiang, J. W. McBride, A nano-indentation study of the contact resistance and resistivity of a bi-layered Au/multi-walled carbon nanotube composite. *Applied Physics Letters*, 2015, **106**(10), Article number 101911.
[69] Y. Yoon, G. S. Lee, K. Yoo, J.-B. Lee. Fabrication of a Microneedle/CNT Hierarchical Micro/Nano Surface Electrochemical Sensor and Its In-Vitro Glucose Sensing Characterization. *Sensors*, 2013, **13**, 16672-16681.
[70] E. Gikunoo, A. Abera, E. Woldesenbet, A Novel Carbon Nanofibers Grown on Glass Microballoons Immunosensor: A Tool for Early Diagnosis of Malaria, *Sensors*, 2014, **14**, 14686-14699.
[71] P. Sui, D. Duckworth, G. Weaver, Joints comprising carbon nanoforests. US Patent 2015/0204444 A1, 2015.
[72] J. H. Taphouse, T. L. Bougher, V. Singh, P. P. S. S. Abadi, S. Graham, B. A. Cola, G. W. Woodruff, Carbon nanotube thermal interfaces enhanced with sprayed on nanoscale polymer coatings, *Nanotechnology*, 2013, **24**(10), Article number 105401.
[73] D. Luo, L. Wu, J. Zhi, Fabrication of Boron-Doped Diamond Nanorod Forest Electrodes and Their Application in Nonenzymatic Amperometric Glucose Biosensing. *ACS Nano*, 2009, **3**(8), 2121–2128.
[74] M. G. Gong, Y. Z. Long, X. L. Xu, H. D. Zhang, B. Sun, Synthesis, Superhydrophobicity, Enhanced Photoluminescence and Gas Sensing Properties of ZnO Nanowires, In: *Nanowires - Recent Advances*, Edited by X. Peng, INTECH, 2012, 77-100.
[75] K. Govatsi, S. N. Yannopoulos, Controlling the morphology of ZnO nanostructures grown by Au catalyzed chemical vapor deposition and chemical bath deposition methods, *Proceedings of the Advanced Architectures in Photonics*, 2014, **1**, 22-26.
[76] X. Sun, Q. Li, J. Jiang, Y. Mao, Morphology-tunable synthesis of ZnO nanoforest and its photoelectrochemical performance, *Nanoscale*, 2014, **6**, 8769-8780.
[77] S. Hwan Ko, D. Lee, H. Wook Kang, K. Hyun Nam, J. Yeob Yeo, S. Joon Hong, C. P. Grigoropoulos, H. Jin Sung. Nanoforest of Hydrothermally Grown Hierarchical ZnO Nanowires for a High Efficiency Dye-Sensitized Solar Cell, *Nano Lett*. 2011, **11**, 666–671.
[78] S. Wang, C. Song, K. Cheng, S. Dai, Y. Zhang, Z. Du. Controllable growth of ZnO nanorod arrays with different densities and their photoelectric properties. *Nanoscale Research Letters*, 2012, **7**, 246.
[79] R. P. Sugavaneshwar, K. K. Nanda, Multistage effect in enhancing the field emission behaviour of ZnO branched nanostructures, *Applied Physics Letters*, 2014, **104**(22), Article number 222104.
[80] P. N. Dave, P. R. Malpani, ZnO nanoforest based new generation dye sensitized solar, *Materials Science Forum*, 2014, **771**, 71-89.
[81] S. Kim, M. Kim, T. Kim, H. Baik, K. Lee, Evolution of space-efficient and facet-specific ZnO 3-D nanostructures and their application in photocatalysis, *Cryst. Eng. Comm*. 2013, **15**(14), 2601-2607.
[82] X. Wang, S. Xie, J. Liu, S. O. Kucheyev, Y. Morris Wang, Focused-ion-beam Assisted Growth, Patterning, and Narrowing the Size Distributions of ZnO Nanowires

for Variable Optical Properties and Enhanced Non-mechanical Energy Conversion. LLNL-JRNL-600673, *Chem. Mater.*, 2013, **25**(14), 2819–2827.

[83] M. A. M. Versteegh, R. E. C. van der Wel, J. I. Dijkhuis. Measurement of light diffusion in ZnO nanowire forests, *Appl. Phys. Lett.*, 2012, **100**, 101108.

[84] X. Sun, Q. Li, Y. Lüc, Y. Mao. Three-dimensional ZnO@MnO_2 Core@shell Nanostructures for Electrochemical Energy Storage, *Chem. Commun*., 2013, **49**, 4456-4458.

[85] P. Gondoni, M. Ghidelli, F. Di Fonzo, A. Li Bassi, C. S. Casari. Fabrication of Nano-engineered Transparent Conducting Oxides by Pulsed Laser Deposition, *Journal of Visualized Experiments*, 2013, **72**, e50297, 1-8.

[86] Y. Pan, G. Hong, S. N. Raja, S. Zimmermann, M. K. Tiwari, D. Poulikakos, Significant thermal conductivity reduction of silicon nanowire forests through discrete surface doping of germanium. *Appl. Phys. Lett*. 2015, **106**, 093102.

[87] A. Cao, E. J. R. Sudhölter, L. C. P. M. de Smet. Silicon Nanowire-Based Devices for Gas-Phase Sensing, *Sensors*, 2014, **14**, 245-271.

[88] G. Pennelli, Top-down fabrication of silicon nanowire devices for thermoelectric applications: properties and perspectives, *Eur. Phys. J. B*, 2015, **88**, 121.

[89] M.-L. Seol, J.-H. Ahn, J.-M. Choi, S.-J. Choi, Y.-K. Choi, Self-Aligned Nanoforest in Silicon Nanowire for Sensitive Conductance Modulation, *Nano Lett*. 2012, **12**, 5603−5608.

[90] M.-L. Seol, J.-M. Choi, J.-Y. Kim, J.-H. Ahn, D.-Il Moon, Y.-K. Choin, Piezoelectric nanogenerator with a nanoforest structure. *Nano Energy*, 2013, **2**, 1142–1148.

[91] D. Aradilla, D. Gaboriau, G. Bidan, P. Gentile, M. Boniface, D. Dubal, P. Gómez-Romero, J. Wimberg, T. J. S. Schubert, S. Sadki, An innovative 3-D nanoforest heterostructure made of polypyrrole coated silicon nanotrees for new high performance hybrid micro-supercapacitors, *Journal of Materials Chemistry A*, 2015, **3**(26), 13978-13985.

[92] L. Zhang, J. He, X. Huang, D. Zhao, D. Zhang, Size-controllable fabrication of nano-to-microstructures on silicon surface using high-density ion etching with pulsed bias, *Micro and Nano Letters*, 2014, **9**(9), 588-591.

[93] A. D. Bao, H. Y. Mao, J. J. Xiong, Z. J. Chen, W. Ou, D. P. Chen, Nanopillar-forest based surface-enhanced Raman scattering substrates, *Sci. China*, 2014, **57**, 082407:1–082407:8.

[94] C. Liu, J. Tang, H. Ming Chen, B. Liu, P. Yang. A Fully Integrated Nanosystem of Semiconductor Nanowires for Direct Solar Water Splitting, *Nano Lett*. 2013, **13**, 2989−2992.

[95] C.-M. Lin, Y.-C. Chang, J. Yao, C. Wang, C. Luo, S. Yin, Multi-step hydrothermally synthesized TiO_2 nanoforests and its application to dye-sensitized solar cells, *Materials Chemistry and Physics*, 2012, **135**(2-3), 723-727.

[96] P. Cheng, Y. Liu, P. Sun, S. Du, Y. Cai, F. Liu, J. Zheng, G. Lu, Hydrothermally growth of novel hierarchical structures titanium dioxide for high efficiency dye-sensitized solar cells, *Journal of Power Sources*, 2014, **268**, 19-24.

[97] F. Shao, J. Sun, L. Gao, Songwang Yang and Jianqiang Luo. Forest-like TiO_2 hierarchical structures for efficient dye-sensitized solar cells. *J. Mater. Chem*., 2012, **22**, 6824–6830.

[98] S. Kannan Balasingam, M. Gu Kang, Y. Jun, Metal substrate based electrodes for flexible dye-sensitized solar cells: fabrication methods, progress and challenges. *Chem. Commun*., 2013, **49**, 11457—11475.

[99] J. An, W. Guo, T. Ma, Enhanced Photoconversion Effi ciency of All-Flexible Dye-Sensitized Solar Cells Based on a Ti Substrate with TiO_2 Nanoforest Underlayer. *Small*, 2012, **8**(22), 3427–3431.
[100] M. Cabello, G. F. Ortiz, M. C. López, R. Alcántara, J. R. González, J. L. Tirado, R. Stoyanova, E. Zhecheva, Self-organized sodium titanate/titania nanoforest for the negative electrode of sodium-ion microbatteries, *Journal of Alloys and Compounds*, 2015, **646**, 816-826.
[101] Y. Li, Y. Zhang, Y. Li, Z. Wang, H. Fu, X. Zhang, Y. Chen, H. Zhang, X. Li, Unveiling the dynamic capacitive storage mechanism of Co_3O_4@$NiCo_2O_4$ hybrid nanoelectrodes for supercapacitor applications, *Electrochimica Acta*, 2014, **145**, 177–184.
[102] W. E. Mahmoud, T. Al-Harbi, Hydrothermal synthesis of ultra fine β-$Co(OH)_2$ nanowires with novel morphologies using supercritical water, *Materials Letters*, 2011, **65**, 1986–1988.
[103] R. Ghosh, M. Kyle Brennaman, T. Uher, M.-R. Ok, E. T. Samulski, L. E. McNeil, T. J. Meyer, R. Lopez, Nanoforest Nb_2O_5 Photoanodes for Dye-Sensitized Solar Cells by Pulsed Laser Deposition, *ACS Appl. Mater. Interfaces*, 2011, **3**, 3929–3935.
[104] G. Ren, M. N. Ferdous Hoque, X. Pan, J. Warzywoda, Z. Fan. Vertically aligned VO_2(B) nanobelt forest and its three-dimensional structure on oriented graphene for energy storage. *J. Mater. Chem. A*, 2015, **3**, 10787–10794.
[105] J. He, Y. Wang, Y. Feng, X. Qi, Z. Zeng, Q. Liu, W. Shan Teo, C. Lip Gan, H. Zhang, H. Chen, Forest of Gold Nanowires: A New Type of Nanocrystal Growth, *ACS Nano*, 2013, **7**(3), 2733–2740.
[106] A. La Porta, M. Grzelczak, L. M. Liz-Marzan, Gold Nanowire Forests for SERS Detection, *Chemistry Open*, 2014, **3**, 146–151.
[107] Y. Liu, Y. Xu, Y. Zhu, J. N. Culver, C. A. Lundgren, K. Xu, C. Wang, Tin-coated viral nanoforests as sodium-ion battery anodes, *ACS Nano*, 2013, **7**(4), 3627-3634.
[108] C.-T. Lin, M.-H. Shiao, M.-N. Chang, N. Chu, Y.-W. Chen, Y.-H. Peng, B.-H. Liao, H. J. Huang, C.-N. Hsiao, F.-G. Tseng, A facile approach to prepare silicon-based Pt-Ag tubular dendritic nano-forests (tDNFs) for solarlight-enhanced methanol oxidation reaction, *Nanoscale Research Letters*, 2015, **10**, 74, 8 pp.
[109] T. Ngoc Huan, D. V. Shinde, S. Kim, S.-H. Han, V. Arterob, H. Chung. Forest of Pt–Au–Ag tri-metallic nanodendrites as an efficient electrocatalyst for methanol oxidation reaction. *RSC Adv.*, 2015, **5**, 6940–6944.
[110] A. P. Dabkowska, C. S. Niman, G. Piret, H. Persson, H. P. Wacklin, H. Linke, C. N. Prinz, T. Nylander, Fluid and Highly Curved Model Membranes on Vertical Nanowire Arrays, *Nano Lett*. 2014, **14**, 4286−4292.
[111] D. C. Watson, R. V. Martinez, Y. Fontana, E. Russo-Averchi, M. Heiss, A. Fontcuberta i Morral, G. M. Whitesides, M. Lončar. Nanoskiving Core−Shell Nanowires: A New Fabrication Method for Nano-optics, *Nano Lett*. 2014, **14**, 524−531.
[112] L. Adler-Abramovich, E. Gazit. The physical properties of supramolecular peptide assemblies: from building block association to technological applications. *Chem. Soc. Rev.*, 2014, **43**, 6881-6893.
[113] S. Scanlon, A. Aggeli. Self-assembling peptide Nanotubes. *NanoToday*, 2008, **3**(3-4), 22-30.
[114] J. Jeon, C. E. Mills, M. Scott Shell, Molecular insights into diphenylalanine nanotube assembly: all-atom simulations of oligomerization, *J. Phys. Chem. B*, 2013, **117**(15), 3935–3943.

[115] L. Adler-Abramovich, M. Badihi-Mossberg, E. Gazit, J. Rishpon. Characterization of Peptide-Nanostructure-Modified Electrodes and Their Application for Ultrasensitive Environmental Monitoring. *Small*, 2010, **6**(7), 825–831.
[116] M. Wang, W. Zhang, Y. Liu, Y. Yang, C. Wang, Y. Wang, Electrochemical performance of patterned $LiFePO_4$ nano-electrode with a pristine amorphous layer. *Applied Physics Letters*, 2014, **104**(17), Article number 171604.
[117] H. Mao, D. Wu, W. Wu, J. Xu, Y. Hao, The fabrication of diversiform nanostructure forests based on residue nanomasks synthesized by oxygen plasma removal of photoresist, *Nanotechnology*, 2009, **20**, 445304, 6 pp.
[118] J. Yeo, S. H. Ko, Hierarchical nanostructures for solar cells, *RSC Nanoscience and Nanotechnology*, 2015, Volume 2015 (35), 2015, 59-83.
[119] C. Liu, J. J. Gallagher, K. K. Sakimoto, E. M. Nichols, C. J. Chang, M. C. Y. Chang, P. Yang, Nanowire−Bacteria Hybrids for Unassisted Solar Carbon Dioxide Fixation to Value-Added Chemicals, *Nano Lett*. 2015, **15**, 3634−3639.
[120] A. P. Dabkowska, C. S. Niman, G. Piret, Henrik Persson, H. P. Wacklin, H. Linke, C. N. Prinz, T. Nylander, Fluid and Highly Curved Model Membranes on Vertical Nanowire Arrays, *Nano Lett.*, 2014, **14**(8), 4286–4292.
[121] L. Wang, C. Ortiz, M. C. Boyce, Mechanics of Indentation into Micro- and Nanoscale Forests of Tubes, Rods, or Pillars. *Journal of Engineering Materials and Technology*, 2011, **133**, 011014, 9 pp.
[122] Method for imaging processing of nanorod/nanoneedle forest structure. Patent CN 104310307 A. 2014.

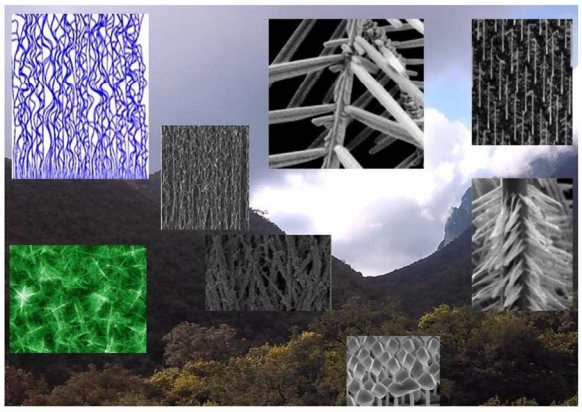

364x186mm (96 x 96 DPI)